^{109}Pd: Difficulties in particle-rotor models for unique-parity states and revision of spectroscopic factors

R. F. Casten, G. J. Smith, M. R. Macphail,* D. Breitig,† W. R. Kane, M. L. Stelts, and S. F. Mughabghab
Brookhaven National Laboratory, Upton, New York 11973

J. A. Cizewski‡
State University of New York, Stony Brook, New York 11794
and Brookhaven National Laboratory, Upton, New York 11973

H. G. Börner, W. F. Davidson, and K. Schreckenbach
Institute Laue Langevin, 38042 Grenoble, France

(Received 5 July 1979)

Primary and secondary γ rays following thermal and p-wave resonant (2.96 eV) neutron capture on ^{108}Pd were measured to study γ-ray transitions in ^{109}Pd. Average resonance capture spectra at 2 and 24 keV were also recorded and the ^{108}Pd$(n,\gamma ce)$ reaction was studied and transition multipolarities were deduced. A detailed level scheme up to $\sim$1400 keV has been constructed. Numerous spin assignments have been revised, leading to substantial changes in the (d,p) and (d,t) spectroscopic factors, in particular for the $g_{7/2}$ orbit. The data on primary transition intensities for the 2.96 eV resonance are compared with the valence neutron capture model. The level scheme deduced for ^{109}Pd sheds new light on the previously proposed $g_{7/2}$-$h_{11/2}$ anomaly in the filling of these orbits, suggesting that, at least in ^{109}Pd, the appearance of the anomaly was largely due to spin misassignments. The revised systematics in the occupation of shell model orbits for a number of nuclei in this mass region is reviewed. Within the level scheme is a group of low-spin negative-parity levels which belong to the same family as the high-spin, decoupled, unique-parity states known in other odd mass Pd isotopes. These states correspond to the favored and unfavored anti-aligned levels for core rotations $R \leq 6$. Calculations in the framework of the particle-rotor model cannot reproduce these level energies.

NUCLEAR REACTIONS ^{108}Pd (n,γ), E=thermal, 2.96 eV, 2 keV, 24 keV; measured E_γ, I_γ, I_γ (θ); ^{108}Pd $(n,\gamma ce)$ ^{109}Pd deduced J, π of 2.96 eV resonance, levels, transitions, multipolarities, J, π. Ge(Li) detectors, three crystal spectrometer, curved crystal spectrometers, conversion electron spectrometer, enriched targets.
NUCLEAR STRUCTURE ^{109}Pd revised (d,p), (d,t) spectroscopic factors, negative-parity anti-aligned favored and unfavored levels, particle-rotor model.

I. INTRODUCTION

An anomaly[1-3] in the filling of certain neutron orbits in the mass region $A = 100$–120 has persisted for a number of years. On the basis of summed (d,p) spectroscopic factors, the $g_{7/2}$ orbit for $A \sim 100$, $Z \sim 46$ nuclei appeared to be nearly *empty* and the presumably higher lying $h_{11/2}$ orbit appeared to be nearly *full*. This $g_{7/2}$-$h_{11/2}$ anomaly is in contrast to the more predictable behavior of the isotonic and heavier Sn nuclei. Table I summarizes the anomaly in terms of the values for $\Sigma S(d,p)$ quoted in Ref. 3. Although the anomaly has been discussed[1,3] both in terms of a breakdown in the basic assumptions of distorted-wave Born approximation (DWBA) stripping theory and of the existence of deformed states in these isotopes, it has never satisfactorily been explained and remains an impediment to a proper understanding of this mass region.

The Pd nuclei play a crucial role in assessing the validity of this $g_{7/2}$-$h_{11/2}$ anomaly. The original (d,p) experiments[1,3] were performed at 12 MeV on Pd, Cd, In, and Sn nuclei. At 17 MeV, however, the anomaly essentially disappears[3] for Cd and persists only in the odd-odd nucleus ^{116}In and in ^{107,109}Pd. Furthermore, in the latter nuclei, the angular distributions for some of the states assigned as $\frac{7}{2}^+$ do not display consistent $l=4$ character.

The odd mass Pd isotopes are also of considerable interest because of the existence of a group of negative parity states based on the unique-parity $h_{11/2}$ orbit. A set of high-spin negative-parity levels, described as the favored, aligned yrast levels forming a decoupled band[4] arising from the coupling of the $h_{11/2}$ orbit to a slightly deformed prolate core, has been identified[5-8] in the lighter odd mass Pd isotopes. Three high-spin unfavored levels were also disclosed.[7-9] A

TABLE I. The $g_{7/2}$-$h_{11/2}$ anomaly.

	Summed (d,p) spectroscopic factors[a]				
	^{107}Pd	^{109}Pd	^{113}Sn	^{115}Sn	^{119}Sn
$g_{7/2}$	0.86	0.76	0.31	0.16	0.16
$h_{11/2}$	0.29	0.28	0.88	0.83	0.70

[a] Quoted in Ref. 3. Note that larger values of $\Sigma S(d,p)$ imply emptier orbits.

prediction of both the decoupled band model and of the weak coupling picture is that not only high-spin, but low-spin negative-parity levels should occur. These should be the favored or unfavored, *anti-aligned* couplings of the schematic form $h_{11/2} \otimes (-\vec{R})$. Only a handful[9-12] of such anti-aligned states has yet been identified, and never the complete set.

The (n,γ) reaction provides, by virtue of its inherent nonselectivity, an appropriate spectroscopic tool for locating these low-spin unique-parity levels and for independently assigning spin values to the positive-parity levels in order to shed light on the apparent $g_{7/2}$-$h_{11/2}$ anomaly. We have, therefore, carried out a variety of (n,γ) experiments, with both thermal and epithermal neutrons, and have measured both primary and secondary γ rays in ^{109}Pd. Some of the results, namely the (n,γ)-(d,p) correlations and the $\frac{3}{2}^-$ assignment for the 2.96 eV resonance, were briefly reported earlier,[13] and the implications of the level scheme study for the $g_{7/2}$-$h_{11/2}$ anomaly and the negative-parity states have been summarized.[14] Prior to the inception of the work, only the isomeric (189 keV) transition in ^{109}Pd was known.[15] During the course of these studies, an unpublished work by Franz[16] has become available and, recently, two other β-decay studies[17] have been reported. Most of the present γ-ray placements agree with those of these studies, although in some cases the higher energy precision of the present work rules out proposed placements of Refs. 16 and 17. Our level scheme contains, in addition, many more transitions as well as transition multipolarities and additional information on level spins from the primary transition angular distributions. The principal results stem from the revision of a number of spin-parity assignments, which, in Refs. 16 and 17, were simply adopted from the previous[1,2] charged particle data.

Section II describes the experimental procedures and tabulates the results including the new spectroscopic factors resulting from the revised spin assignments. A brief discussion of the valence neutron capture model is also included. Section III then discusses the implication of the level scheme for the filling of shell model orbits in the region and the consequences of the observed low-lying unique-parity levels for rotation-aligned models.

II. EXPERIMENT

A. Experimental techniques and results

Several independent (n,γ) experiments on ^{108}Pd were performed at the Institute Laue Langevin (ILL) and at Brookhaven National Laboratory (BNL).

1. Experiments at BNL for thermal and 2.96 eV neutron energies

These experiments were carried out in external neutron beams provided by the Brookhaven National Laboratory High Flux Beam Reactor (HFBR). In all of these, the γ rays were detected with Ge(Li) detectors of various sizes. Typical resolutions were 7 keV at $E_\gamma = 6$ MeV. The Ge(Li) detector calibrations were obtained with standard sources and a precision pulser, and by use of known contaminant lines from Al and Fe for the higher energy transitions. The experiments consisted of the following:

(a) Detection of both high energy (primary) and low energy (secondary) γ rays following thermal neutron capture and capture in the 2.96 eV p-wave resonance.

(b) For the p-wave resonance, the anisotropy of the more intense primary transitions was measured at 90° and 135° to the beam direction.

(c) An off-resonance measurement of 2.0 eV was performed to detect contaminant and background γ rays.

The thermal neutron beam was provided by a quartz filter which eliminated pile γ rays and fast neutrons. The thermal flux on target was approximately $7 \times 10^7 (n/\text{cm}^2)/\text{sec}$. The HFBR neutron monochromator facility[18] provided the resonance energy neutrons via Bragg diffraction from a large Be crystal. The target consisted of 5.52 grams

TABLE II. Anisotropy of γ rays from a $p_{3/2}$ resonance for zero target spin. (See Ref. 19.)

Transition	$W(\theta)$	$\frac{I_\gamma(90°)}{I_\gamma(135°)}$
$\frac{3}{2} \rightarrow \frac{1}{2}$	$\frac{1}{16\pi}(2 + 3\sin^2\theta)$	1.43
$\frac{3}{2} \rightarrow \frac{3}{2}$	$\frac{1}{20\pi}(7 - 3\sin^2\theta)$	0.73
$\frac{3}{2} \rightarrow \frac{5}{2}$	$\frac{3}{80\pi}(6 + \sin^2\theta)$	1.08

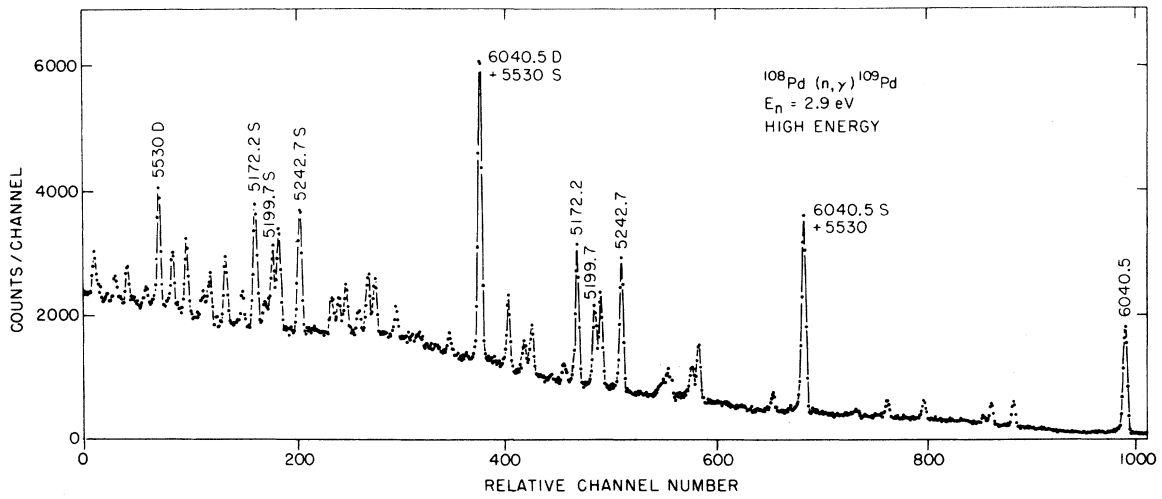

FIG. 1. Portion of a spectrum of high energy capture γ rays from the ^{108}Pd$(n,\gamma)^{109}$Pd reaction on the 2.96 eV resonance in the compact geometry. A few of the peaks are labeled according to energy. The letters *S* and *D* following a photopeak energy denote single and double escape peaks, respectively.

enriched to 98.11% in ^{108}Pd and formed into a rectangle approximately 2.54 cm × 2.86 cm. The target was normally mounted at ~45° to the beam direction but this was changed to ~30° for the angular distribution measurements in order to reduce differences in γ-ray self-absorption for the different detector angles.

To determine the neutron separation energy for ^{109}Pd, only accurately measured primary transitions to well-defined levels were used. From the thermal neutron data a separation energy of 6153.7 ± 0.5 keV was deduced from 10 primary transitions, and a value of 6154.1 ± 0.4 keV was obtained from 15 resonance primary transitions. Combining the two results gives a neutron separation energy of 6154.0 ± 0.3 keV, in agreement with the value 6151 ± 8 keV tabulated in Ref. 19.

In these experiments, all but the weakest primary γ rays are almost certainly dipole in character. Thus, in thermal capture ($\frac{1}{2}^+$ capture state), these transitions directly populate $J=\frac{1}{2}$, $\frac{3}{2}$ final states. In a $\frac{3}{2}^-$ resonance, as the 2.96 eV resonance was determined to be, $J=\frac{1}{2}$, $\frac{3}{2}$, $\frac{5}{2}$ states are populated by anisotropic dipole primary transitions whose intensity ratio $I_\gamma(90°)/I_\gamma(135°)$ is spin dependent; Table II lists the ratios for each final state spin. The ratio for a $J=\frac{5}{2}$ state is intermediate between those for $J=\frac{1}{2}$ and $\frac{3}{2}$ states,

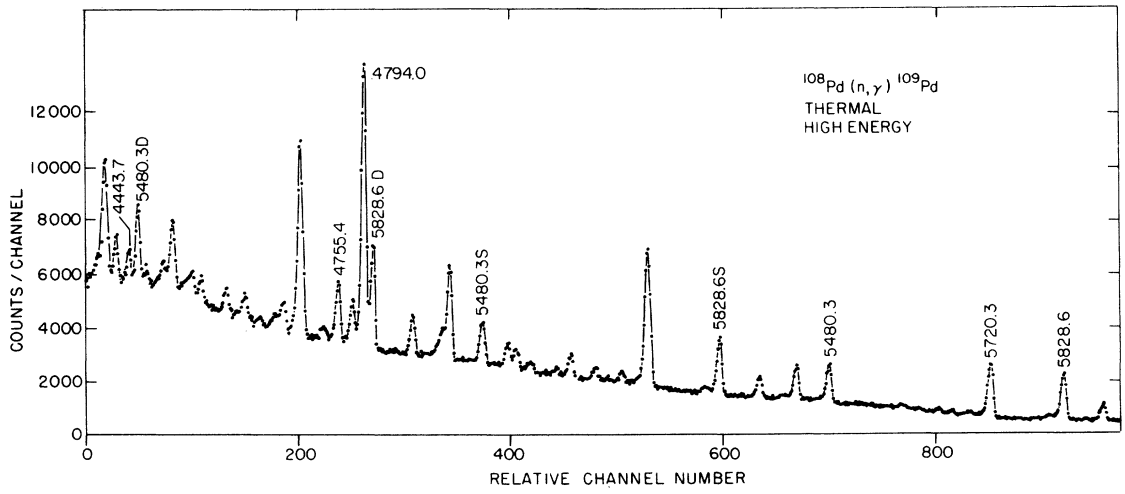

FIG. 2. Portion of a spectrum of high energy thermal capture γ rays from the ^{108}Pd$(n,\gamma)^{109}$Pd reaction. The notation on selected peaks follows the convention given in the caption to Fig. 1.

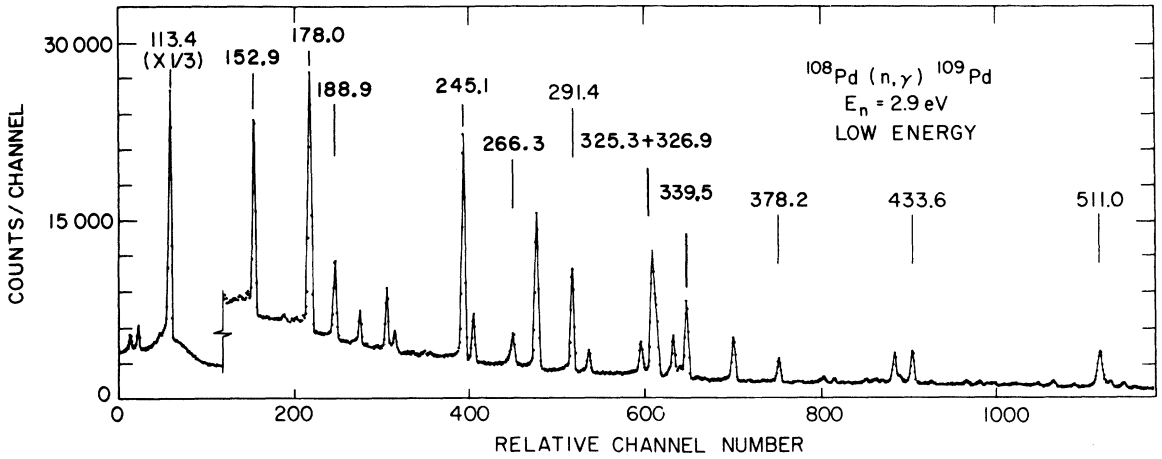

FIG. 3. Portion of a spectrum of low energy γ rays following neutron capture on ^{108}Pd in the 2.96 eV resonance. A few reference γ-ray energies are given above their respective peaks.

which themselves differ by a factor of almost 2. In most cases where experimental uncertainties in the ratios are relatively large, the $J=\frac{5}{2}$ assignment will remain a possibility. However, the observation of a strong primary transition to such a level in thermal capture would exclude this assignment.

Figures 1 and 2 show spectra of primary transi-

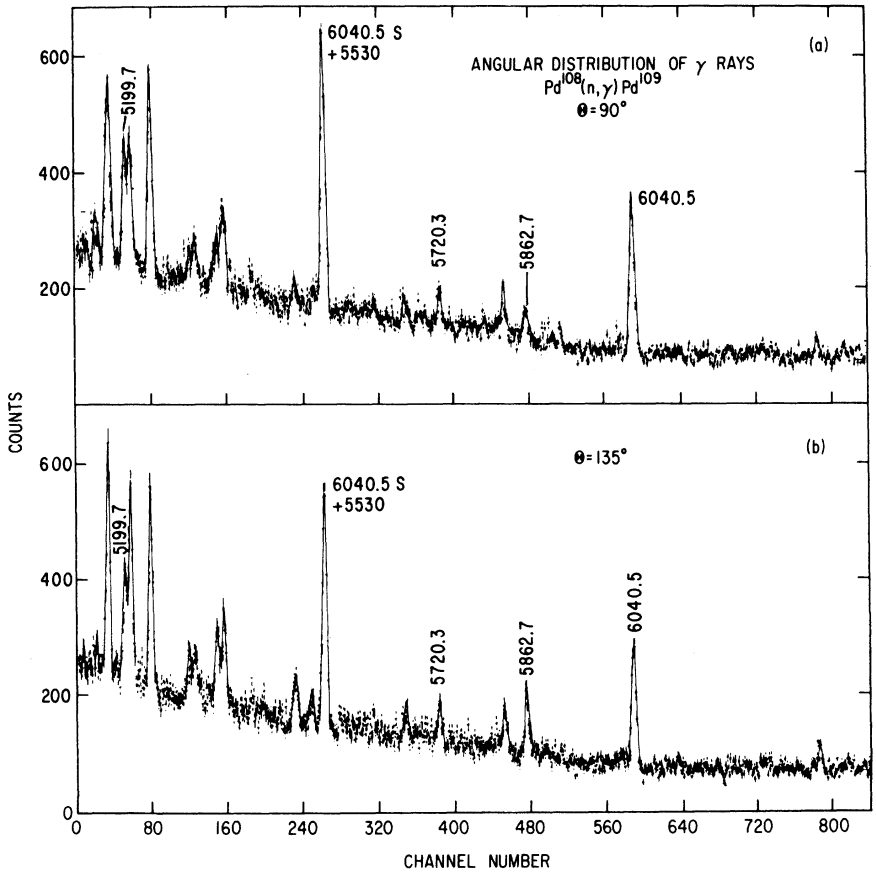

FIG. 4. Portions of spectra recorded on the 2.96 eV resonance in the angular distribution geometry at angles of 90° and 135° to the incident beam direction. Typical energy labels are affixed to some peaks according to the notation described in the caption to Fig. 1.

tions for the 2.96 eV resonance and for thermal energy, respectively, while Fig. 3 shows a portion of the low energy γ-ray spectrum following resonance capture. Figure 4 is an example of part of the primary spectrum recorded in the angular distribution geometry.

To determine the absolute intensities of primary γ rays, measurements of known decay γ rays were performed after the neutron irradiations. For the ^{109}Pd case, we considered the 309.1, 311.4, and 647.3 keV decay γ rays ($\tau_{1/2}$ = 13.46 h), whose intensities are 4.9, 31.9, and 24.4 gamma rays/10^5 ^{109}Pd decays.[20] For thermal capture, the absolute intensity of the strongest primary γ ray in

TABLE III. Primary γ-ray transitions for the ^{108}Pd(n,γ) ^{109}Pd reaction at E_n = 2.96 eV.

E_γ (keV)[a]	E_{ex} (keV)[b]	I_γ[c] Photons/1000 neutron captures	$\frac{I_\gamma(90°)}{I_\gamma(135°)}$[d]	J[e]
6154(4)	g.s.	0.6(2)		
6040.5	113.4	33.6	1.42 ± 0.06	$\frac{1}{2}$
5862.7	291.2	7.5(8)	0.73 ± 0.07	$\frac{3}{2}$
5827.2	326.7	6.5(7)	$0.81^{+0.20}_{-0.08}$	$\frac{3}{2}, \frac{5}{2}$[f]
5815.0	338.9	2.1(2)		
5720.3	433.6	4.7(5)	0.80 ± 0.15	$\frac{3}{2}$ ($\frac{5}{2}$)
5662.3	491.6	4.4(5)		
5612.6	541.3	1.7(4)		
5530(3)	624(2)	12.8(13)	0.87 ± 0.09	$\frac{3}{2}, \frac{5}{2}$
5508.0	645.9	1.0(4)		
5480.6	673.3	4.7(6)		
5362.6	791.3	13.1(13)	1.04 ± 0.07	$\frac{5}{2}$
5307(4)	847(3)	1.3(6)		
5242.7	911.2	28.2(23)	1.08 ± 0.04	$\frac{5}{2}$
5209.1	944.9	16.1(16)	0.77 ± 0.06	$\frac{3}{2}$
5199.7	954.3	17.8(18)	1.19 ± 0.08	$\frac{1}{2}, \frac{5}{2}$
5172.2	981.8	29.5(28)	1.09 ± 0.06	$\frac{5}{2}$
5100.0	1054.0	9.1(13)	0.99 ± 0.20	$\frac{5}{2}$ ($\frac{3}{2}$)
5063.0	1091.0	15.7(13)	$1.00^{+0.05}_{-0.09}$	$\frac{5}{2}$
4884.2	1269.8	5.1(6)		
4825.6	1328.4	4.4(5)	0.43 ± 0.25[g]	($\frac{3}{2}$)[g]
4795.5	1358.5	4.4(13)		
4782.9	1371.1	7.2(6)	1.03 ± 0.15	$\frac{5}{2}$
4754.8	1399.1	0.6(2)		
4676.4	1477.6	5.1(5)		
4613.7	1540.3	12.1(10)	0.82 ± 0.07	$\frac{3}{2}$
4530.1	1623.9	9.1(10)		
4506.2	1647.8	6.3(10)		

[a] The γ-ray energy uncertainty is ±1.5 keV unless otherwise specified. The larger uncertainties (given in parentheses on the last digit) result from the overlapping of full energy peaks of some transitions with escape peaks of others.

[b] Level energy uncertainties are ±0.5 keV unless otherwise specified. The excitation energy scale assumes an energy of 113.4 keV for the state populated by the 6040.5 keV primary transition.

[c] Absolute intensities at 90° in the compact geometry. Uncertainties in parentheses on the last digits are relative only. In addition, the absolute intensity scale (i.e., intensity of the 6040.5 keV γ ray) is accurate to ±24%.

[d] The quantity R gives the fully corrected ratio of primary intensities obtained from the runs at 90° and 135° with the Ge(Li) counter more distant from the target.

[e] The J values are those spin assignments that can be made from the angular distribution results alone. See text for discussion and Table VIII for best J^π values from all the data.

[f] There is a doublet at 325–326 keV. The measured primary energy suggests that the 326 keV level is populated on resonance but the impossibility of ruling out some contribution from the other level precludes making a reliable distinction of spins from the data in this table.

[g] This spin suggestion is tentative due to the large statistical uncertainties of the peaks involved.

^{109}Pd ($E_\gamma = 4794.0$ keV) was determined to be 68.3 ± 7.8 photons/1000 neutron captures, which is in disagreement with a value of 30.0 photons/1000 neutron captures derived from measurements of Rasmussen *et al.*[21] based on thermal capture cross sections of 6.1 ± 0.4 and 8.3 ± 0.6 b,[22] respectively, for Pd and ^{108}Pd.

To verify several weak $E2$ primary transitions following thermal capture, a separate study of primary transitions employing a three crystal pair spectrometer[23] was performed on a Bi filtered beam line. For this experiment a target of 7.7 g enriched to 98.11% in ^{108}Pd was used. The experimental facility has been described elsewhere.[23]

Table III summarizes the primary γ-ray data for the 2.96 eV resonance. It includes all primary transitions observed, their absolute intensities, the intensity ratio at 90° and 135° for the stronger transitions, and the level spins deduced from the angular anisotropy measurement alone. Table IV presents the energies and absolute intensities of primary transitions for thermal capture. Table V presents the data for secondary transitions up to 1019.9 keV following both thermal and resonance capture. The resonance intensities result from the Ge(Li) measurements alone while secondary γ-ray energies and thermal capture intensities result from a combination of Ge(Li) detector measurements at BNL and the curved crystal spectrometer data from ILL discussed in the next section. Average resonance capture experiments were also performed at BNL but are more suitably discussed later.

TABLE IV. Primary γ-ray transitions for the ^{108}Pd(n,γ) ^{109}Pd reaction at thermal energy.[a]

E_γ (keV)	E_{ex} (keV)	I_γ Photons/1000 neutron captures
6152.9	g.s.	1.1(2)
5887.5	266.3	7.5(14)
5828.6	325.2	19.1(20)
5720.3	433.5	21.2(20)
5661.9	491.5	1.8(13)
5612.9	540.5	0.9(4)
5480.3	673.5	12.9(14)
5431.7	722.1	11.7(14)
5211.8	942.0	27.4(28)
5171.6	981.8	3.0(12)
5099.7	1054.1	7.5(6)
5041.6	1111.8	2.5(11)
5018.9	1134.9	5.8(6)
5006.1	1147.7	6.4(6)
4920.3	1233.5	17.8(20)
4909.5	1243.9	4.3(15)
4885.3(11)	1268.1(10)	0.7(4)[b]
4794.0	1359.8	68.3
4775.7	1378.1	11.7(42)
4755.4	1398.4	15.7(41)
4674.1	1479.7	6.6(15)
4668.5	1484.9	2.1(4)[b]
4616.5	1537.3	5.1(25)
4552.1	1601.7	6.0(15)
4538.0	1615.8	6.5(19)
4509.2	1644.6	10.9(41)
4469.9	1683.5	4.2(17)
4443.7	1710.2	7.5(28)

[a] All uncertainties are denoted in parentheses and are on the last digit of the corresponding entry. For γ-ray energies, the uncertainties are ±0.8 keV unless otherwise specified. The excitation energy scale is obtained by taking 673.5 keV as the energy of the state fed by the 5480.3 keV primary transition. Excitation energies are accurate to ±0.5 keV unless specified. The uncertainties on intensities are relative only; the absolute intensity scale (defined by the intensity of the 4794.0 keV γ ray) is accurate to ±12%.

[b] Observed only in the thermal measurement with the three crystal spectrometer; below sensitivity limit in the other thermal measurement.

2. *Experiments performed at the ILL*

The study of low energy γ rays in ^{109}Pd with extremely high energy precision (typically 2–25 eV) and resolution was performed with GAMS 1 and GAMS 2/3 curved crystal spectrometers which have been described elsewhere.[24] The target was an in-pile laminar sample of ~70 mg of enriched ^{108}Pd situated in a flux of 5.5×10^{14} (n/cm^2)/sec. The low energy γ rays emitted following neutron capture pass out of the reactor along a transverse beam tube and are diffracted by the curved crystals of GAMS 1 and GAMS 2/3 which are located at opposite ends of a through tube. The thinner GAMS 1 crystal is suitable for the study of γ rays up to ~500 keV while GAMS 2/3 may be best used in the energy range 200–1200 keV.

Corresponding portions of a GAMS 2 and a Ge(Li) spectrum are contrasted in Fig. 5. (Note that the energy dispersion and resolution in third through fifth order reflections in GAMS are better than those shown but the reflectivities are lower.) The GAMS data were energy calibrated internally by demanding that a line have the same energy in all orders of reflection in which it is observed. Absolute energy calibration is performed by reference to the 88.034 keV ^{109}Ag line.[25]

Since the GAMS target is viewed end on by the spectrometers, the self-absorption corrections can be large. For this reason the adopted intensities for the low energy γ rays were obtained by plotting the ratio of Ge(Li) intensities to those measured by the GAMS spectrometers, and by using the values for strong transitions to define a relative effective GAMS efficiency curve (including

TABLE V. Low energy secondary gamma rays for the reaction ^{108}Pd(n,γ) ^{109}Pd.

E_γ (keV)[a]	I_γ[b] (γ's/1000 neutron captures) Thermal	2.96 eV	Assignment
94.450(1)	34.7(35)	15.4(15)	339 → 245
98.258(3)	16.5(17)	21.8(22)	(287 → 189)[c]
106.694(3)	1.0(2)	0.8(3)	434 → 327
108.280(1)	4.9(6)	2.1(3)	(434 → 325)[d]
113.401(2)	297(30)	187(19)	113 → 0
149.854(3)	1.0(1)	1.8(2)	426 → 276
152.942(1)	95.2(95)	41.9(42)	266 → 113
166.306(4)	2.2(4)	1.9(4)	492 → 325
170.561(1)	2.4(2)	2.9(6)	
178.034(1)	72.0(72)	61.1(61)	291 → 113
187.115(4)	1.0(1)	...	811 → 623
188.990(1)	16.5(17)	19.2(19)	189 → 0
189.920(3)	2.8(4)	2.6(4)	623 → 434
197.333(8)	0.6(1)	0.6(3)	623 → 426
200.153(4)	12.0(12)	9.8(10)	492 → 291
202.971(13)	0.3(1)	0.7(2)	
207.697(3)	0.3(1)	0.7(2)	
211.884(3)	33.6(34)	17.7(18)	325 → 113
213.806(4)	1.8(3)	1.4(2)	541 → 327
215.390(2)	6.7(7)	5.9(6)	541 → 325
216.487(9)	0.5(1)	0.3(2)	
222.922(6)	0.6(1)	0.8(3)	945 → 782
224.717(7)	0.6(1)	...	1359 → 1135
228.194(4)	0.7(1)	1.7(2)	
230.453(2)	2.8(3)	1.4(2)	722 → 492
245.080(2)	154(15)	82.7(83)	245 → 0
249.238(11)	19.4(19)	17.8(18)	541 → 291
263.403(6)	2.0(4)	0.6(4)	
264.378(11)	1.4(4)	0.9(8)	541 → 276
264.980(3)	13.4(13)	5.6(6)	604 → 339
266.346(3)	27.5(28)	12.9(13)	266 → 0
267.610(5)	2.2(4)	...	941 → 673
274.328(7)	0.6(1)	0.7(2)	541 → 266
276.296(5)	32.6(33)	69.6(70)	276 → 0
288.480(5)	2.2(3)	1.3(3)	722 → 434
291.430(4)	60.3(60)	49.9(50)	291 → 0
295.597(3)	1.4(3)	0.8(2)	541 → 245
298.197(5)	12.6(13)	10.6(11)	623 → 325
299.119(5)	1.9(3)		
317.255(6)	1.8(4)	1.1(3)	(604 → 287)[c]
320.164(5)	27.8(28)	17.2(17)	434 → 113
321.082(15)	0.9(5)	...	
325.284(4)	122(12)	70.5(71)	325 → 0
326.868(4)	48.9(49)	40.5(41)	327 → 0
332.050(5)	3.2(6)	3.2(4)	623 → 291
333.964(3)	64.1(64)	24.6(25)	673 → 339
336.584(3)	21.0(21)	6.0(6)	941 → 604
337.828(5)	1.2(3)	0.9(5)	
339.528(4)	114(11)	50.0(50)	339 → 0
343.869(9)	1.9(4)	1.5(3)	
346.622(6)	0.6(1)	1.0(2)	673 → 327
347.192(6)	1.8(3)		623 → 276
355.694(6)	1.5(5)	...	
357.148(9)	0.6(1)	...	623 → 266
358.697(10)	8.5(11)	31.9(32)	
359.426(6)	68.7(69)		604 → 245
365.295(7)	0.6(3)	0.8(2)	791 → 426
371.125(10)	2.4(4)	1.4(3)	
377.004(13)	1.8(3)	0.6(3)	811 → 434

TABLE V. (*Continued*).

E_γ (keV) [a]	I_γ [b] (γ's/1000 neutron captures) Thermal	2.96 eV	Assignment
378.191(5)	24.3(24)	17.7(18)	492 → 113
386.752(40)	1.1(3)	...	
392.395(25)	0.4(1)	...	
395.171(17)	2.9(4)	1.8(3)	722 → 327
396.758(11)	10.2(10)	5.1(5)	722 → 325
407.124(10)	1.5(4)	1.6(3)	
414.342(7)	6.0(6)	4.0(4)	
416.738(20)	0.4(1)	1.4(3)	
418.298(7)	1.8(3)	3.5(4)	
421.049(11)	1.5(3)	3.2(3)	
426.135(4)	11.7(12)	27.1(27)	426 → 0
428.396(3)	19.0(19)	7.1(7)	673 → 245
433.552(4)	58.9(59)	32.4(32)	434 → 0
436.185(11)	0.6(1)	...	
438.160(12)	1.4(3)	...	
441.839(9)	2.3(5)	3.2(5)	
452.524(16)	0.8(1)	...	
455.702(5)	7.7(8)	4.2(4)	722 → 266
461.194(7)	13.1(13)	4.0(4)	1135 → 673
464.541(9)	1.6(3)	2.5(4)	791 → 327
466.511(10)	2.2(5)	3.2(4)	
467.333(12)	1.0(5)		
485.311(7)	5.1(6)	3.0(4)	811 → 325
491.575(10)	9.6(10)	7.0(7)	492 → 0
515.128(13)	5.7(8)	7.1(7)	791 → 276
520.597(10)	4.3(6)	6.7(7)	954 → 434
525.078(16)	1.4(3)	2.6(6)	791 → 266
526.411(21)	0.5(1)	1.7(6)	
530.202(10)	2.6(4)	0.9(6)	1135 → 604
539.345(31)	0.6(3)	1.7(15)	
540.697(10)	3.1(7)	2.6(14)	541 → 0
554.589(44)	0.8(3)	4.6(5)	
555.614(13)	1.8(3)		982 → 426
566.672(20)	0.4(3)	...	
579.896(30)	0.8(3)	1.3(3)	
584.505(51)	0.5(2)	2.7(4)	911 → 327
585.908(15)	1.5(3)		
601.575(6)	15.6(18)	3.9(4)	941 → 339
604.530(6)	5.5(7)	2.6(4)	604 → 0
608.672(9)	1.8(4)	1.7(3)	
612.047(12)	2.1(4)	1.2(3)	
619.939(28)	5.4(9)	8.9(9)	(911 → 291) [d]
620.441(16)	5.2(8)		
623.468(16)	6.2(10)	5.0(5)	623 → 0
628.887(18)	2.7(4)	3.0(4)	954 → 325
632.363(18)	1.6(3)	1.1(3)	
634.907(23)	2.9(5)	8.2(8)	
645.963(44)	0.8(3)	1.4(4)	
649.650(29)	0.5(2)	...	941 → 291
653.504(36)	0.8(3)		945 → 291
654.892(16)	1.9(4)	5.5(6)	982 → 327
655.501(16)	3.1(5)		
657.569(29)	4.4(5)	6.4(6)	
660.128(31)	0.6(3)	...	
670.089(58)	0.7(4)	...	
673.607(40)	1.0(3)	1.3(3)	(673 → 0) [e]
674.725(30)	3.0(4)		941 → 266

TABLE V. (*Continued*).

E_γ (keV) [a]	I_γ [b] (γ's/1000 neutron captures) Thermal	2.96 eV	Assignment
678.040(35)	1.6(3)	4.1(4)	791 → 113
678.673(41)	1.2(3)		945 → 266
680.968(33)	1.8(3)	2.0(3)	
685.909(24)	22.8(23)	3.4(3)	1359 → 673
690.300(26)	4.4(5)	15.3(15)	982 → 291
695.949(32)	2.2(3)	0.8(3)	941 → 245
705.433(47)	0.8(3)	2.5(4)	982 → 276
711.400(56)	1.3(4)	...	
713.389(20)	3.8(5)	4.1(4)	
722.025(27)	14.0(14)	6.8(7)	722 → 0
726.740(24)	5.5(6)	5.1(6)	1054 → 327
754.908(22)	26.7(27)	3.2(4)	1359 → 604
772.096(20)	4.4(6)	1.3(3)	
787.314(34)	2.3(5)	1.5(3)	1054 → 266
791.429(31)	3.5(5)	4.8(5)	791 → 0
793.570(23)	3.4(5)	1.8(3)	
799.265(51)	5.1(6)	4.1(4)	(1233 → 434) [d]
810.547(13)	14.5(22)	7.4(7)	(811 → 0) [e]
815.228(24)	3.6(8)	2.8(3)	
820.242(25)	3.3(7)	1.8(3)	
831.571(15)	11.7(18)	18.2(18)	945 → 113
840.759(27)	4.6(14)	5.7(6)	954 → 113
846.328(13)	11.1(28)	15.8(16)	
902.981(38)	3.4(5)	...	
911.283(24)	4.0(7)	14.4(14)	911 → 0
966.439(24)	7.8(8)	1.9(4)	(1233 → 266) [d]
1019.868(27)	12.5(13)	1.7(3)	1359 → 339

[a] All uncertainties are denoted in parentheses and are on the last digit(s) of the corresponding entry. The observed gamma-ray energies are obtained from the curved-crystal spectrometer experiments.

[b] All uncertainties are denoted in parentheses and are on the last digit(s) of the corresponding entry. The intensities are obtained from the Ge(Li) spectrometer experiments for both neutron energies with the exception that several thermal intensities, in particular for very weak or multiplet lines, are obtained by scaling the curved-crystal spectrometer data to the Ge(Li) spectrometer data. There is an absolute intensity scale uncertainty of 15% for the thermal data and 25% for the 2.96 eV data.

[c] Placement is tentative since the 287 keV level is not definitely known to exist.

[d] Placement is tentative. Ratio of thermal to resonance γ-ray intensities is in poor agreement with the average ratio for other γ rays depopulating this state.

[e] Placement is tentative. Energy combination is worse than $3\sigma_{E_\gamma}$ compared to the average energy combination of other γ rays depopulating this state.

automatically the self-absorption correction) and by using this curve to normalize all GAMS intensities to the Ge(Li) intensity scale.

The other measurements performed at the ILL consisted of the study of the $(n,\gamma ce)$ reaction with the electron spectrometer BILL.[26] These data are used, alone and in conjunction with the γ-ray data, to provide transition multipolarities for nearly all strong transitions below 450 keV. The BILL spectrometer detects electrons, emitted from an in-pile target, in a multiwire gas counter. The target consisted of an evaporated film of thickness 150 μg/cm^2 enriched in ^{108}Pd with dimensions 3 cm × 10 cm. Typical resolution was $\Delta E/E \approx 10^{-3}$. In addition to a complete repetition of the entire electron energy range, the regions 320–325 and 400–410 keV were scanned repeatedly (35 times for the latter) in order to detect the weak $L1$ electrons from the 325 keV transition and to detect and resolve the K electrons for the transitions of 426, 428, and 433 keV. As a result, the energy and intensity uncertainties for these electron transitions were considerably reduced. Three small portions of an electron spectrum are shown in Fig. 6.

The electron energies were calibrated with the use of the accurately known GAMS energies by using a least squares fit to selected strong lines.

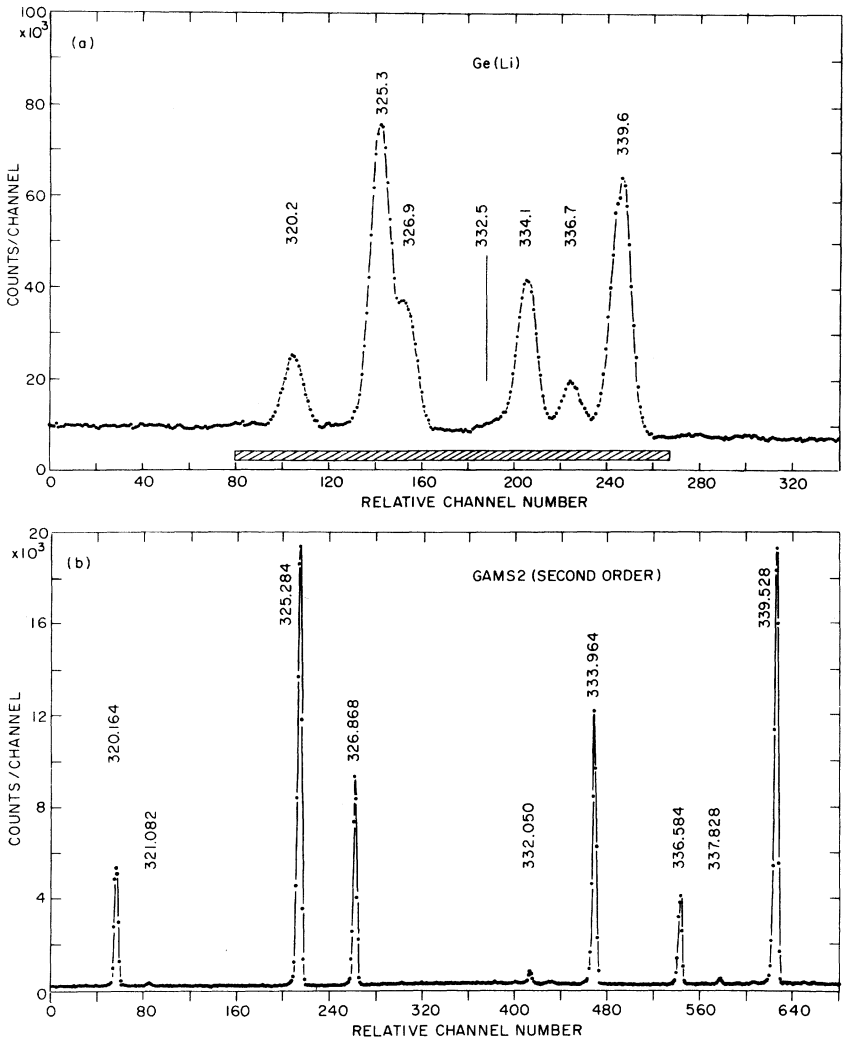

FIG. 5. Comparison of portions of a Ge(Li) spectrum (a) and a GAMS2 spectrum (b) in second order following thermal capture. The shaded bar at the bottom of the Ge(Li) spectrum shows the γ-ray energy region spanned by the GAMS2 spectrum below it. Note that the GAMS dispersion (and therefore energy precision) is greater for higher order of reflection.

The absolute intensity scale was established by demanding that the 152.9 and 266.3 keV transitions from the 266.3 keV ($\frac{1}{2}^+$) level to the 113.4 keV ($\frac{1}{2}^+$) and 0 keV ($\frac{5}{2}^+$) levels be pure $M1$ and $E2$, respectively. This normalization is justified by a consistent set of spin assignments for other levels, and since it yields an $E2$ multipolarity for the 113-0 ($\frac{1}{2}^+ \rightarrow \frac{5}{2}^+$) transition and an $E3$ multipolarity for the known isomeric transition of 189 keV.

Table VI shows the results of these measurements including, in the last column, the adopted multipolarities. In many cases these were determined from the ratios of electron to γ-ray intensities. In a number of others, however, the ratios of conversion electron intensities from different shells or subshells provide an independent determination. In particular, one notes the drastic effects of a small $E2$ admixture on the L and M subshell ratios. This sensitivity allowed the small $E2$ admixture in the 94 keV transition to be identified and shows, for example, that, to high accuracy, the 113 keV transition is pure $E2$.

Nearly all transitions studied appear to be of pure multipolarity; the only definite exception being that of 94 keV. For two others (264 and 276 keV) small admixtures of competing multipolarities are tentatively suggested (with large errors), while for others, such admixtures, though not supported by positive evidence, cannot be rigorously excluded. For these cases the formally allowed possibilities are explicitly noted.

While these results will be discussed in detail

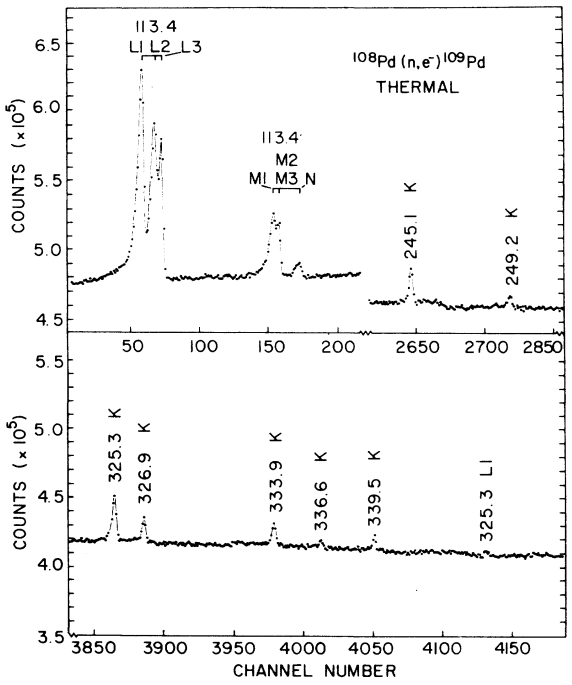

FIG. 6. Portions of the electron spectrum for the reaction ^{108}Pd $(n,\gamma ce)^{109}$Pd. The peaks are labeled by approximate transition energy and by electron subshell. The region shown near the 325.3 keV $L1$ transition was repeatedly scanned in a separate measurement yielding higher accuracy than one would infer from the figure.

below, we stress here the consequence of the $E1$ multipolarity deduced for the 245 keV ground state transition, namely, that it establishes an entire family of negative-parity levels. The $E1$ multipolarity results independently from both the K and L conversion electrons and stems from the low conversion coefficients measured. Careful inspection of the GAMS data in high order of reflection showed that this assignment cannot be due to an unresolved γ-ray doublet at 245 keV; any detected second transition would have to be degenerate to within 20 eV. Furthermore, the parity changing nature of the 245 keV transition is confirmed by the $E1$ assignment for the 339 keV ground state transition and the parity nonchanging $M1+E2$ transition between the 339 and 245 keV levels.

3. *Average capture experiments (BNL)*

From the above data a level scheme was constructed (see Sec. II C) which included negative-parity states at 189, 245, 287, 339, 604, 645, 673, 941, and probably 1359 keV. The spins were, however, not uniquely determined. The high current interest in unique-parity states provided the incentive for more definitive spin assignments and, to this end, we performed average resonance capture measurements at 2 and 24 keV. This technique, given sufficient averaging, enables one to distinguish spin (and parity) values on the basis of differences in the averaged intensity of $E1$ and $M1$ primary transitions following s- and p-wave capture. The technique has been described elsewhere.[28] The experimental apparatus[23] at BNL produces nonmonoenergetic [full width at half maximum (FWHM) ~900 eV] neutron beams of 2 and 24 keV by passing a neutron beam through filters composed primarily of Sc and ^{56}Fe, respectively.

A target of 7.7 g enriched to 98.11% in ^{108}Pd was used. It was approximately 2.5×2.5 cm in size and oriented at 45° to the neutron beam. The γ rays following neutron capture were detected by a three crystal pair spectrometer and calibrated for both energy and intensity by using the accurately known values[23] for the ^{35}Cl$(n,\gamma)^{36}$Cl reaction.

Figure 7 shows the spectrum for 2 keV average capture. Several background lines were observed and have been identified. Spins are indicated for those states whose spins were unambiguously known from the earlier measurements. Table VII is a tabulation of the average capture results.

One does not expect the averaged primary intensities to be constant for a given final state spin but to exhibit a smooth energy dependence of the form E_γ^n, where $n=5$ is usually[28] used. In the present application we are not concerned with this question but only whether or not the intensities lie in a relatively narrow band when plotted against E_γ. (That band need not be horizontal.) For convenience we tabulate the reduced intensities I_γ/E_γ^5; it is these values that should be consulted to inspect the quality of the averaging.

From Table VII, it is apparent that states with $J=\frac{1}{2}, \frac{3}{2}$ are populated at 2 keV with reduced intensities of ~6, that $\frac{5}{2}^+$ levels have populations in the range 1.6–4.1 and that $\frac{5}{2}^-$ levels have intensities of ~1.3. The dominant routes (capture state, primary transition multipolarity) for population of final states with different J^π values are $\frac{1}{2}^+$, $\frac{3}{2}^+$ (p-wave, $E1$ and s wave, $M1$), $\frac{1}{2}^-$, $\frac{3}{2}^-$ (s wave, $E1$ and p wave, $M1$), $\frac{5}{2}^+$ ($p_{3/2}$, $E1$), $\frac{5}{2}^-$ ($p_{3/2}$, $M1$). Thus, the ratio of $\frac{5}{2}^+$ to $\frac{5}{2}^-$ populations gives the averaged intensity ratio for $E1/M1$ for which a value of ~3 is deduced. From this and the approximately equal populations for $\frac{1}{2}$, $\frac{3}{2}$ states regardless of parity, one deduces that the reaction is averaging over approximately equal strengths due to s- and p-wave resonances at 2 keV. From the ±~30% fluctuations in reduced intensities for $J=\frac{1}{2}, \frac{3}{2}$ states, the averaging must then include on the order of ten s- and p-wave resonances. As a check, these results

TABLE VI. Conversion electron measurements following the ^{108}Pd$(n,\gamma ce)^{109}$Pd reaction for thermal neutrons.

E_γ [a] (keV)	E_{e^-} [a] (keV)	Shell	$E_{trans.}$ (keV)	I_γ [a] photons/1000 capture events	I_e [a] electrons/1000 capture events	$\alpha_{Exp.}$	α_{Theory} [b] $M1$	$E1$	$E2$	$E3$	Comments
94.450(1)	70.098(9)	K	94.448	34.7(35)	15.0(23)	0.433(87)	0.391	0.158	1.32		$M1(20\pm10\%\ E2)$
	90.850(11)	$L1$	94.455		1.53(15)	0.044(6)	0.0445	0.0153	0.119		
	91.125(13)	$L2$	94.455		0.486(194)	0.014(6)	0.0028	0.0015	0.0949		
	91.287(11)	$L3$	94.447		0.625(250)	0.018(8)	0.0008	0.0023	0.120		
	93.854(38)	MT	94.454		0.625(250)	0.018(9)	0.0090	0.0035	0.0642		
98.258(3)	73.907(7)	K	98.257	16.5(17)	4.70(71)	0.285(49)	0.349	0.141	1.15		$M1$
	94.653(11)	$L1$	98.258		0.726(145)	0.044(10)	0.0397	0.0137	0.104		
113.401(2)	89.054(9)	K	113.404	297(30)	166(17)	0.559(78)	0.234	0.0931	0.708		$E2$
	109.792(7)	$L1$	113.397		15.7(16)	0.053(8)	0.0266	0.0092	0.0655		
	110.071(7)	$L2$	113.401		9.21(92)	0.031(4)	0.0016	0.0008	0.0399		
	110.226(7)	$L3$	113.396		11.6(12)	0.039(6)	0.0005	0.0012	0.0483		
	112.736(7)	$M1$	113.406		2.97(30)	0.010(2)	0.0050	0.0017	0.0119		
	112.760(7)	$M2, M3$	113.410		4.16(42)	0.014(2)	0.0004	0.0004	0.0174		
152.942(1)	128.592(7)	K	152.942	95.2(95)	9.04(45)	0.095(10)	0.102	0.0395	0.252		$M1$ [d]
	149.335(9)	$L1$	152.940		0.952(95)	0.010(2)	0.0116	0.0040	0.0242		
	152.309(16)	MT	152.909		0.190(32)	0.002(5)	0.0023	0.0009	0.0086		
178.034(1)	153.684(2)	K	178.034	72.0(72)	4.54(14)	0.063(6)	0.0678	0.0257	0.148		$M1$
	174.435(8)	$L1$	178.040		0.432(86)	0.006(1)	0.0077	0.0026	0.0146		
188.990(1)	164.635(3)	K	188.985	16.5(17)	8.32(25)	0.504(50)	0.0579	0.0217	0.121	0.574	$E3$
	185.382(4)	$L1$	188.987		0.809(81)	0.049(7)	0.0066	0.0022	0.0119	0.0544	
	185.662(5)	$L2$	188.992		0.908(136)	0.055(9)	0.0003	0.0001	0.0037	0.0634	
	185.815(5)	$L3$	188.986		0.759(114)	0.046(8)	0.0001	0.0002	0.0039	0.0570	
	188.420(9)	MT	189.020		0.363(73)	0.022(5)	0.0013	0.0005	0.0037	0.0339	
200.153(4)	175.798(8)	K	200.148	12.0(12)	0.492(103)	0.041(10)	0.0497	0.0184	0.0990		$M1(\leq3\%\ E2)$
211.884(3)	187.533(3)	K	211.883	33.6(34)	1.48(6)	0.044(5)	0.0427	0.0157	0.0814		$M1$
	208.287(12)	$L1$	211.892		0.235(71)	0.007(2)	0.0048	0.0016	0.0082		
215.390(2)	191.039(11)	K	215.389	6.7(7)	0.261(26)	0.039(5)	0.0409	0.0150	0.0769		$M1(\leq9\%\ E2)$
245.080(2)	220.727(5)	K	245.077	154(15)	1.54(5)	0.010(1)	0.0292	0.0105	0.0497		$E1$
	241.510(15)	$L1$	245.115		0.231(46)	0.0015(3)	0.0033	0.0011	0.0051		
249.238(11)	224.897(6)	K	249.247	19.4(19)	0.524(42)	0.027(3)	0.0280	0.0100	0.0470		$M1(\leq11\%\ E2)$
264.980(3)	240.642(9)	K	264.992	13.4(13)	0.402(60)	0.030(5)	0.0239	0.0085	0.0382		$M1(43\pm35\%\ E2)$
266.346(3)	242.001(4)	K	266.351	27.5(28)	1.10(3)	0.040(4)	0.0236	0.0083	0.0376		$E2$ [d]
276.296(5)	251.948(6)	K	276.298	32.6(33)	0.782(23)	0.024(2)	0.0215	0.0076	0.0333		$M1(21\pm17\%\ E2)$
291.430(4)	267.076(8)	K	291.426	60.3(60)	1.27(4)	0.021(2)	0.0187	0.0066	0.0279		$M1$
	287.821(78)	$L1$	291.426		0.241(120)	0.004(2)	0.0021	0.0007	0.0029		
298.197(5)	273.813(18)	K	298.162	12.6(13)	0.239(72)	0.019(6)	0.0177	0.0062	0.0258		$M1(16^{+74}_{-16}\%\ E2)$
320.164(5)	295.809(9)	K	320.159	27.8(28)	0.361(65)	0.013(3)	0.0148	0.0051	0.0205		$M1(\leq21\%\ E2)$
325.284(4)	300.927(4)	K	325.277	122(12)	1.83(6)	0.015(1)	0.0142	0.0049	0.0194		$M1(15^{+20}_{-15}\%\ E2)$
	321.847(30)	$L1$	325.452		0.244(41)	0.002(1)	0.0016	0.0005	0.0020		
326.868(4)	302.514(7)	K	326.864	48.9(49)	0.978(39)	0.020(2)	0.0140	0.0048	0.0192		$E2(\leq23\%\ M1)$
333.964(3)	309.595(8)	K	333.945	64.1(64)	0.897(27)	0.014(1)	0.0133	0.0046	0.0179		$M1(15^{+22}_{-15}\%\ E2)$

TABLE VI. (*Continued*).

E_γ [a] (keV)	E_{e^-} [a] (keV)	Shell	$E_{trans.}$ (keV)	I_γ [a] photons/1000 capture events	I_e [a] electrons/1000 capture events	α_{Exp}	α_{Theory} [b] *M1*	*E1*	*E2*	*E3*	Comments
336.584(3)	312.215(10)	*K*	336.564	21.0(21)	0.273(19)	0.013(2)	0.0130	0.0045	0.0174		*M*1(≤45 % *E*2)
339.528(4)	315.171(7)	*K*	339.521	114(11)	0.570(57)	0.005(1)	0.0127	0.0044	0.0169		*E*1(1^{+2}_{-1} % *M*2)
359.426(6)	335.067(6)	*K*	359.417	68.7(69)	0.687(27)	0.010(1)	0.0110	0.0038	0.0142		*M*1 [e]
378.191(5)	353.821(12)	*K*	378.171	24.3(24)	0.292(58)	0.012(3)	0.0097	0.0033	0.0120		*E*2(≤100 % *M*1)
426.135(4)	401.779(37)	*K*	426.129	11.7(12)	0.064(16)	0.0055(20)	0.0072	0.0025	0.0083		*M*1(≲27 % *E*2) [f]
428.396(5)	404.058(23)	*K*	428.408	19.0(19)	0.152(15)	0.008(1)	0.0071	0.0024	0.0082		*E*2(≤100 % *M*1)
433.552(4)	409.217(12)	*K*	433.567	58.9(59)	0.383(31)	0.0065(8)	0.0069	0.0024	0.0079		*M*1(≤40 % *E*2)

[a] Uncertainties are denoted in parentheses and are on the last digit(s) of the corresponding entry. The intensity uncertainties are relative only. The absolute intensity scale is accurate to ±15%.

[b] Theoretical conversion ratio values are calculated according to the prescription of Ref. 27.

[c] The limits or values given for competing multipolarities assume the full extent of the listed uncertainties in α_{exp} and thus are probably conservative overestimates. Where electrons from more than one shell or subshell are observed the deduced multipolarities utilize the ratios of electron intensities in addition to comparisons with γ-ray intensities.

[d] The 266.343 keV level is assigned $J^\pi = \frac{1}{2}^+$. Thus, the 152.942 and 266.346 keV transitions must be pure *M*1 and pure *E*2, respectively. These two transitions were used as the calibration points for the conversion electron data.

[e] α_{Exp} is also consistent with an assignment of *E*1 (16 ± 3% *M*2).

[f] α_{Exp} is also consistent with an assignment of *E*1 (13 ± 9% *M*2).

then give approximately the correct ratio of $\frac{5}{2}^+$ to $J = \frac{1}{2}, \frac{3}{2}$ population as well. Known levels that are not observed most likely have $J \geq \frac{7}{2}$. (The possibility of $\frac{5}{2}^-$ cannot be rigorously excluded since such states seem to be populated near the limit of sensitivity and there is an insufficient number of them known to verify precisely the degree of averaging.) Table VII gives the spin restrictions directly implied by the average capture data. When combined with the results of the other experiments, the average capture data allows a substantial refinement of the adopted spin set. Note also that the nonobservance of the 370, 382, 404, 742, and 960 keV levels, all but the last observed very weakly in Refs. 1–3, implies either that they do not exist or else have spins $\frac{5}{2}^-$ or $\geq \frac{7}{2}$.

B. Spin of the 2.96 eV resonance

The spin and parity of the 2.96 eV resonance were not known prior to the inception of this study. The current experiment demonstrates that it is a $p_{3/2}$ resonance. This is clear from the fact that the intensity ratios [$I(90/I(135)$] in Table III are not all unity, and in particular by their strong variation from transition to transition. The fact that several previously assigned $\frac{5}{2}^+$ states are populated by primary transitions provides additional support.

C. Level scheme for ^{109}Pd

Figure 8 shows the level scheme for ^{109}Pd for excitation energies below 1.36 MeV based upon the present data. The construction of the level scheme was based upon precise energy combinations and by the requirement that the ratio of the intensities of γ rays depopulating each level observed in thermal capture and in the 2.96 eV resonance must be constant to within the intensity uncertainties. Levels were introduced into the level scheme only when defined by three or more primary and secondary transitions. (Exceptions to this rule are the well known[15] $\frac{11}{2}^-$ isomer at 189 keV and the 287 and 1233 keV levels which are discussed below.) Figure 8 includes, as short horizontal bars, a number of levels for which no depopulation has been determined. These levels are, however, populated by primary γ rays in the thermal and/or 2.96 eV resonance reactions as indicated.

The curved crystal spectrometer efficiency falls off rapidly with increasing γ-ray energy so that these data are primarily of use for $E_\gamma < 1$ MeV. Since the level scheme relies on precise Ritz combinations, Ge(Li) data alone were not used and, therefore, Table V terminates at $E_\gamma \sim 1020$ keV. Owing to this restriction, the level scheme

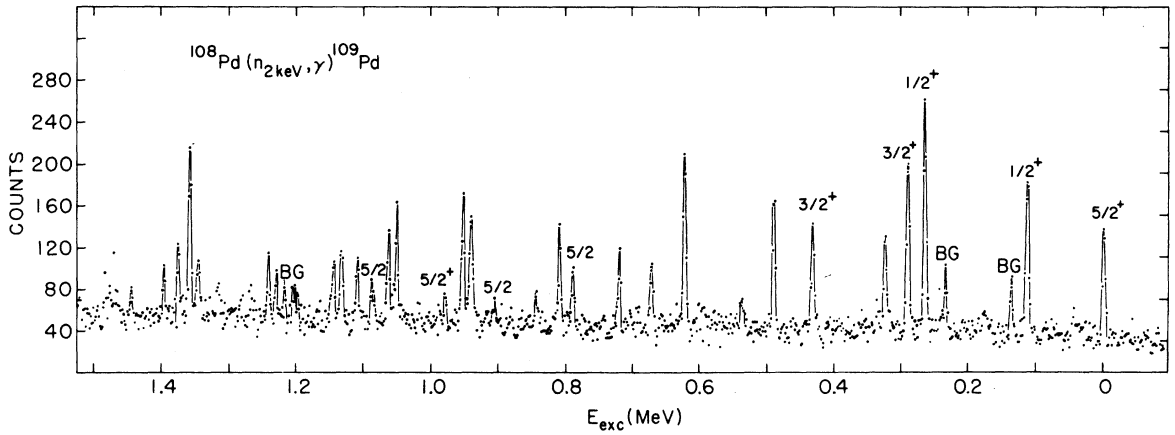

FIG. 7. A portion of the spectrum of double escape peaks for $E_n = 2$ keV average resonance capture. Peaks corresponding to states with unambiguous spins based upon data from the other experiments are labeled. Background peaks are denoted by BG.

may be incomplete above ~1 MeV in that transitions to the ground state region may not have been placed. (An exception is the 1359 keV level for which special attention has been given to such transitions as will be discussed below.)

Spin and parity assignments are made on the basis of the thermal and resonance primary γ-ray data, the resonance angular anisotropy measurement, the $(n,\gamma ce)$ data, and the average capture data. Population by a primary transition restricts the possible spin assignments for a level, since such transitions have dipole multipolarity, except for the weakest which may be $E2$. Thus, primary population of a low-lying state in the $\frac{3}{2}^-$ resonance implies a final state spin of $\frac{1}{2}$, $\frac{3}{2}$, $\frac{5}{2}$, $(\frac{7}{2}^-)$ and in thermal capture a spin of $\frac{1}{2}$, $\frac{3}{2}$, $(\frac{5}{2}^+)$ where the J^π values in parentheses are those allowed for $E2$ primary transitions. The population of some states by strong primary transitions in both thermal and resonance capture (with capture states of opposite parity) demonstrates that $M1$ transitions can be comparable to the strongest $E1$ primary transitions in this mass region. Thus, parity assignments cannot be made on the basis of primary transition intensities in the thermal or single resonance capture experiments.

For all levels observed, Table VIII gives the adopted level energies and J^π assignments and summarizes the earlier charged particle transfer work. In addition, and in lieu of a detailed description of each level, the table succinctly summarizes the arguments for the J^π values. A few specific points are explicitly mentioned below either where the level is particularly important for later discussion, or the argument is complex, or where ambiguities remain.

245.081(2) keV; $\frac{7}{2}^-$ $(\frac{5}{2}^-)$. From the $E1$ multipolarity of the 245 keV γ ray, this level must be $\frac{3}{2}^-$, $\frac{5}{2}^-$, $\frac{7}{2}^-$. The average capture data exclude the $\frac{3}{2}^-$ choice and argue strongly against the $\frac{5}{2}^-$ choice leaving $\frac{7}{2}^-$ as the most likely spin. This negative-parity assignment, which is in sharp disagreement with the $\frac{7}{2}^+$ value given in Refs. 1, 2, 16, and 17, has considerable impact on both the resolution of the $g_{7/2}$-$h_{11/2}$ anomaly and on the identification of negative-parity states. (See Sec. III.)

Owing to the importance of the negative-parity assignment, we show the evidence for the $E1$ multipolarity assignment more explicitly in Fig. 6. Shown there are the K conversion lines from the 245 keV $E1$ and 249 keV $M1$ transitions; the K conversion coefficients are 0.010 ± 0.001 and 0.027 ± 0.003, respectively. This difference of a factor of almost 3 is just the difference in $M1$ and $E1$ K conversion coefficients for Pd at 250 keV.

287.250(3) keV; $\frac{9}{2}^-$. The existence of this level is tentative as only two secondary γ rays can be placed to define it. The 317 keV γ ray depopulates the 604 keV level while the 98 keV $M1$ γ ray populates the 189 keV level. The latter restricts the possible spin assignments $\frac{9}{2}^-$, $\frac{11}{2}^-$, $\frac{13}{2}^-$. However, the transition from the 604 keV level ($J = \frac{5}{2}$, see below) rules out $\frac{11}{2}^-$ or $\frac{13}{2}^-$. Thus, if the state exists, it is $J^\pi = \frac{9}{2}^-$. A possible third transition to define this level is that depopulating the 645 keV level. This transition is plausible but not shown in Fig. 8 since an insufficient number of combinations involving the 645 keV level were found to precisely determine the energy of that level.

326.869(2) keV; $\frac{5}{2}^+$. The multipolarity of the 326 keV γ ray is $E2$, so the parity for this level is positive and the transition from the 673 keV level ($J^\pi = \frac{3}{2}^-$) rules out $\frac{7}{2}^+$ for the 326 keV level.

TABLE VII. Results of the average resonance capture experiments.

E_{ex} [a] (keV)	I_γ/E_γ^5 (MeV^{-5}) [b] E_n=2 keV	E_e=24 keV	J^π [c]
0	4.1(4)	0.1(1)	$\frac{5}{2}^+$
113.400	7.2(6)	1.4(2)	$\frac{1}{2},\frac{3}{2}$
188.990	···	···	$\geq\frac{7}{2}$
245.081	$\leq$1.1(3) [d]	0.2(2)	$(\frac{5}{2}^-), \geq\frac{7}{2}$
266.343	10.2(7)	1.2(2)	$\frac{1}{2},\frac{3}{2}$
276.290	···	···	$\geq\frac{7}{2}$
287.250	···	···	$\geq\frac{7}{2}$
291.434	8.2(8)	1.6(2)	$\frac{1}{2},\frac{3}{2}$
325.285	4.8(5)	1.9(3)	both $\frac{5}{2}$ or $\frac{5}{2}^+$
326.869			and $\frac{1}{2},\frac{3}{2}$
339.530	1.2(4)	0.2(1)	$\frac{5}{2}^-$
426.140	$\leq$1.1(4) [d]	···	$(\frac{5}{2}^-), \geq\frac{7}{2}$
433.562	5.4(5)	0.9(3)	$\frac{1}{2},\frac{3}{2}$
491.590	7.1(7)	0.4(2)	$\frac{1}{2},\frac{3}{2}$
540.676	1.6(4)	1.9(3)	$\frac{5}{2}^+$
604.513	1.3(4)	0.4(2)	$\frac{5}{2}^-$
623.482	10.5(9)	1.6(3)	$\frac{1}{2},\frac{3}{2}$
645.9	···	0.3(2)	$\frac{5}{2}^-, \geq\frac{7}{2}$
673.491	4.8(6)	0.9(3)	$\frac{1}{2},\frac{3}{2},(\frac{5}{2}^+)$
722.043	4.0(6)	1.0(2)	$\frac{1}{2},\frac{3}{2},\frac{5}{2}^+$
791.426	4.1(7)	1.4(3)	$\frac{1}{2},\frac{3}{2},\frac{5}{2}^+$
810.595	5.9(7)	0.8(3)	$\frac{1}{2},\frac{3}{2}$
846.1	2.3(5)	0.7(4)	$\frac{5}{2}^+$
911.303	1.9(5)	0.9(3)	$\frac{5}{2}$
941.100	5.5(18)	1.3(3)	both $\frac{1}{2},\frac{3}{2}$
944.967	5.4(18)		
954.163	9.3(9)	0.7(3)	$\frac{1}{2},\frac{3}{2}$
981.755	1.8(6)	0.7(3)	$\frac{5}{2}$
1053.628	8.0(10)	1.5(4)	$\frac{1}{2},\frac{3}{2}$
1065.8	6.6(9)	1.1(3)	$\frac{1}{2},\frac{3}{2}$
1091.0	3.5(7)	1.6(4)	$\frac{5}{2}^+$
1111.8	5.9(9)	1.2(4)	$\frac{1}{2},\frac{3}{2}$
1134.696	7.8(10)	0.8(4)	$\frac{1}{2},\frac{3}{2}$
1147.7	5.4(9)	2.0(5)	$\frac{1}{2},\frac{3}{2}$
1232.795	4.2(9)	$\leq$2.6(5) [d]	$\frac{1}{2},\frac{3}{2},\frac{5}{2}^+$
1243.9	5.1(10)	1.9(5)	$\frac{1}{2},\frac{3}{2}$
1269.5	3.3(8)	1.1(5)	$\frac{1}{2},\frac{3}{2},\frac{5}{2}^+$
1328.4	1.6(9)	1.2(6)	$\frac{5}{2}$
1347.7	$\leq$6.5(12) [d]	2.0(6)	$\frac{1}{2},\frac{3}{2},\frac{5}{2}^+$

TABLE VII. *(Continued)*

E_{ex} [a] (keV)	I_γ/E_γ^5 (MeV^{-5}) [b] E_n=2 keV	E_n=24 keV	J^π [c]
1359.413	19.4(19)	1.3(5)	$\frac{1}{2},\frac{3}{2}$
1371.1	···	1.2(6)	$\geq\frac{5}{2}$
1378.1	7.4(13)	0.8(6)	$\frac{1}{2},\frac{3}{2}$
1399.0	5.5(11)	1.3(7)	$\frac{1}{2},\frac{3}{2}$

[a] Excitation energies listed are those obtained by combining all experimental data, not just that of the average capture measurements. An excitation energy cutoff of 1.4 MeV was enforced as the sensitivity decreased appreciably at approximately this energy.

[b] Relative reduced intensities with errors in parentheses on the last digit. The reduced intensities employ different arbitrary scales for the two neutron energies. Direct comparison of entries can only be made within a column, not between columns.

[c] The J^π values listed are those deduced *solely* from the average capture data. Unless explicitly noted the parity of a state is not assigned, i.e., an entry of $\frac{3}{2}$ means $\frac{3}{2}^\pm$. The following guide lines were employed in making spin assignments: $J^\pi=\frac{1}{2}^\pm,\frac{3}{2}^\pm$, $I_\gamma/E_\gamma^5 \gtrsim 4$ at 2 keV and $I_\gamma/E_\gamma^5 \gtrsim 1$ at 24 keV; $J^\pi=\frac{5}{2}^+$, $1.6 \lesssim I_\gamma/E_\gamma^5 \lesssim 4$ at 2 keV and $0.7 \lesssim I_\gamma/E_\gamma^5 \lesssim 2$ at 24 keV; $J^\pi=\frac{5}{2}^-$, $I_\gamma/E_\gamma^5 \lesssim 1.5$ at 2 keV and $I_\gamma/E_\gamma^5 \lesssim 0.5$ at 24 keV. There are several instances in which both requirements are not fulfilled, due to poor statistics at E_n=24 keV. For these cases assignments were made based upon the reduced intensities at 2 keV.

[d] Background peak known to exist at approximately the same energy as the primary γ ray. Only an upper limit of the primary γ-ray intensity can be obtained.

The 2 keV average capture intensity to the 325–326 keV doublet is insufficient for there to be two $\frac{3}{2}^+$ levels or a $\frac{3}{2}^+$, $\frac{1}{2}^+$ pair, so the 326 keV level must be $\frac{5}{2}^+$. This is consistent with the angular distribution data for the 2.96 eV resonance. In Ref. 17, an 81 keV transition was placed from this level to the state at 245 keV. If this placement is correct the multipolarity assigned to the transition in Ref. 17 cannot be correct. However, the implied $E1$ multipolarity is consistent with the uncertainties (±86%) on α_k cited in Ref. 17.

604.513(3) keV; $\frac{5}{2}^-$ and 941.100(3) keV; $\frac{3}{2}^-$. The spin arguments for these two levels are unambiguous but complex; we present them in detail. The 604 keV level is defined by at least six secondary transitions. Depopulation to the negative-parity states at 245 and 339 keV by parity non-changing transitions establishes negative parity. The 941 keV level is populated by a strong primary transition in thermal capture indicating that $J=\frac{1}{2}$, $\frac{3}{2}$. One of the six γ rays depopulating the 941 keV level is an $M1$ transition feeding the 604 keV level; thus, the 941 keV state is also negative parity and the 604 keV level must then have $J^\pi=\frac{1}{2}^-$, $\frac{3}{2}^-$, or $\frac{5}{2}^-$.

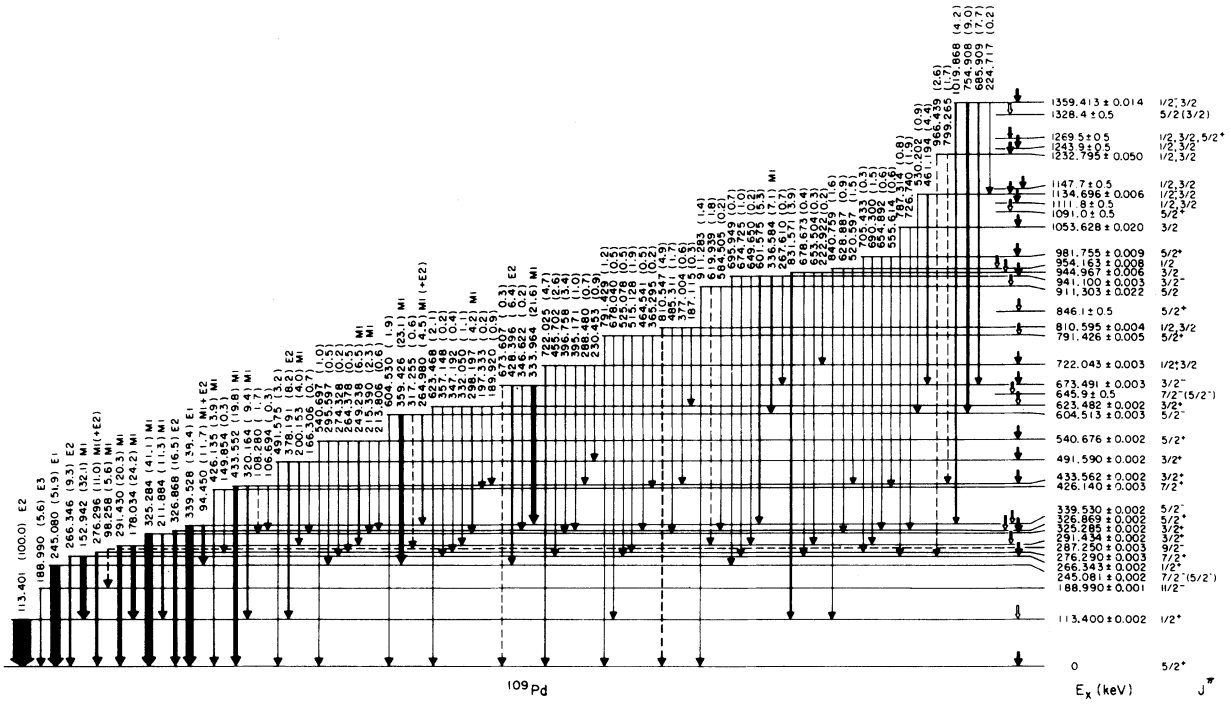

FIG. 8. Level scheme for ^{109}Pd. Relative intensities of secondary γ rays are indicated by arrow thicknesses and are specifically given in parentheses relative to a value of 100 for the 113 keV γ ray. (Intensities are for γ rays and do *not* include correction for internal conversion.) Excitation energies include nuclear recoil corrections. However, energies given above transition arrows are γ-ray energies. Questionable placements of γ rays are indicated by dashed arrows. Short arrows at right indicate primary transitions as follows: open arrow—primary transition observed for 2.96 eV resonance, solid arrow—primary transition observed for thermal capture or for both thermal and resonance capture Finally, J^π assignments which do not specifically show a parity mean that both positive and negative parities are possible, e.g., $J^\pi = \frac{1}{2}$ means $J^\pi = \frac{1}{2}^\pm$. In addition to the levels shown, states at 1065.5 ± 0.5 ($\frac{1}{2}^\pm, \frac{3}{2}^\pm$) and 1347.7 ± 0.5 keV ($\frac{1}{2}^\pm, \frac{3}{2}^\pm, \frac{5}{2}^+$), though not populated by primary transitions in thermal or 2.96 eV capture, are suggested by the average capture results.

Weak population of the latter in average capture implies that $J^\pi = \frac{5}{2}^-$ for the 604 keV level which is also consistent with the $M1$ transition to the likely $\frac{7}{2}^-$ 245 keV state. Given the $\frac{5}{2}^-$ nature of the 604 keV level, the 941 keV state must then be $\frac{3}{2}^-$ as would also be required if the 245 keV level is in fact $\frac{7}{2}^-$.

645.9(5) keV; $\frac{7}{2}^-$ ($\frac{5}{2}^-$). This level is populated by a weak primary γ ray in the 2.96 eV resonance indicating that $J = \frac{1}{2}^\pm, \frac{3}{2}^\pm, \frac{5}{2}^\pm, \frac{7}{2}^-$. No secondary transitions could be unambiguously placed. The average capture results eliminate $\frac{1}{2}^\pm$, $\frac{3}{2}^\pm$, and $\frac{5}{2}^+$ spins. The $\frac{5}{2}^-$ possibility is also unlikely since both the $\frac{5}{2}^-$ levels at 339 and 604 keV are seen in average resonance capture.

673.491(3) keV; $\frac{3}{2}^-$. This state is defined by six secondary transitions and by two primary transitions. The strong thermal primary γ ray indicates a dipole transition and thus $J = \frac{1}{2}, \frac{3}{2}$. The level is depopulated by the 334 keV ($M1$) and 428 keV ($E2$) γ rays to the negative-parity states at 339 and 245 keV, respectively. Both establish negative parity for the 673 keV level and the former gives a unique $\frac{3}{2}^-$ assignment.

1053.628(20) keV; $\frac{3}{2}^\pm$. This level is defined by population by a primary γ ray at both thermal and 2.96 eV neutron energies and by two secondary γ rays which depopulate it. The resonance angular anisotropy measurement favors a spin assignment of $\frac{5}{2}$ over $\frac{3}{2}$. However, the thermal primary intensity is too strong to be $E2$, so that $J = \frac{3}{2}$ would be the more likely assignment. Since the anisotropy is rather poorly defined, this assignment is not inconsistent. It is also supported by the strong population in average resonance capture.

1232.795(50) keV; $\frac{1}{2}^\pm, \frac{3}{2}^\pm$. The two γ rays which depopulate the level of 799.265(51) and 966.439(24) keV give good agreement in their energy combinations. However, the intensity ratio for the 799 keV γ ray is 1.2 ± 0.3, while for the 966 keV γ ray it is 4.0 ± 0.8. Clearly, one or both of these two γ rays does not depopulate this state. In the absence of a third γ ray to establish the intensity ratio for the level, both transitions are considered

TABLE VIII. Summary of information on levels in ^{109}Pd for $E_x \lesssim 1.7$ MeV.

Present work		Previous work [c]			J^π limitations				
E_{ex} (keV) [a] (adopted)	J^π [b] (adopted)	E_{ex} (keV)	l	J^π	From primary transitions (Tables III, IV)	From angular distribution data at 2.96 eV (Table III)	From average Res. Capt. (Table VII)	From secondary transitions [d] and $(n,\gamma ce)$ multipolarities (Tables V and VI) transition	Parity
0	$\frac{5}{2}^+$ [e]	0	2	$\frac{5}{2}^+$	$\frac{1}{2}^\pm, \frac{3}{2}^\pm, \frac{5}{2}^+$		$\frac{5}{2}^+$		
113.400(2)	$\frac{1}{2}^+$	113	0	$\frac{1}{2}^+$	$\frac{1}{2}^\pm, \frac{3}{2}^\pm, \frac{5}{2}^\pm$	$\frac{1}{2}^\pm$	$\frac{1}{2}^\pm, \frac{3}{2}^\pm$	$E2$ to $\frac{5}{2}^+$	+
188.990(1)	$\frac{11}{2}^-$ [e]	188	5	$\frac{11}{2}^-$			$\geq\frac{7}{2}$	$E3$ to $\frac{5}{2}^+$	−
245.081(2)	$\frac{7}{2}^-(\frac{5}{2}^-)$	244	4	$\frac{7}{2}^+$			$(\frac{5}{2}^-), \geq\frac{7}{2}$	$E1$ to $\frac{5}{2}^+$	−
266.343(2)	$\frac{1}{2}^+$ [e]	264	0	$\frac{1}{2}^+$	$\frac{1}{2}^\pm, \frac{3}{2}^\pm$		$\frac{1}{2}^\pm, \frac{3}{2}^\pm$		
276.290(3)	$\frac{7}{2}^+$						$\geq\frac{7}{2}$	$M1(E2)$ to $\frac{5}{2}^+$	+
(287.250(3)	$\frac{9}{2}^-$)						$\geq\frac{7}{2}$	$M1$ to $\frac{11}{2}^-$, fed from $\frac{5}{2}^-$	−
291.434(2)	$\frac{3}{2}^+$	291	2	$\frac{3}{2}^+$	$\frac{1}{2}^\pm, \frac{3}{2}^\pm, \frac{5}{2}^\pm$	$\frac{3}{2}^\pm$	$\frac{1}{2}^\pm, \frac{3}{2}^\pm$	$M1$'s to $\frac{1}{2}^+$ and $\frac{5}{2}^+$	+
325.285(2)	$\frac{3}{2}^+$	324	2	$\frac{3}{2}^+$	$\frac{1}{2}^\pm, \frac{3}{2}^\pm$		(see text)	$M1$'s to $\frac{1}{2}^+$ and $\frac{5}{2}^+$	+
326.869(2)	$\frac{5}{2}^+$				$\frac{1}{2}^\pm, \frac{3}{2}^\pm, \frac{5}{2}^\pm$	$(\frac{3}{2}^\pm, \frac{5}{2}^\pm)$	$\frac{5}{2}^+$ (see text)	$E2$ to $\frac{5}{2}^+$, fed from $\frac{3}{2}^-$	+
339.530(2)	$\frac{5}{2}^-$	339 [f]			$\frac{1}{2}^\pm, \frac{3}{2}^\pm, \frac{5}{2}^\pm, \frac{7}{2}^-$		$\frac{5}{2}^-$	$E1$ to $\frac{5}{2}^+$, $M1(E2)$ to $\frac{7}{2}^-(\frac{5}{2}^-)$	−
Do not exist		370 [g]	(1)	$(\frac{3}{2}^-)$					
or		382 [g]	0, 2	$\frac{1}{2}^+, (\frac{3}{2}^+)$					
$J=\frac{5}{2}^-$ or $\geq\frac{7}{2}$		404 [g]	0	$\frac{1}{2}^+$					
426.140(3)	$\frac{7}{2}^+$	427	4	$\frac{7}{2}^+, (\frac{9}{2}^+)$			$(\frac{5}{2}^-), \geq\frac{7}{2}$	$M1$ to $\frac{5}{2}^+$	+
433.562(2)	$\frac{3}{2}^+$				$\frac{1}{2}^\pm, \frac{3}{2}^\pm$	$\frac{3}{2}^\pm, (\frac{5}{2}^\pm)$	$\frac{1}{2}^\pm, \frac{3}{2}^\pm$	$M1$'s to $\frac{1}{2}^+$ and $\frac{5}{2}^+$	+
491.590(2)	$\frac{3}{2}^+$	490	2	$\frac{3}{2}^+, (\frac{5}{2}^+)$	$\frac{1}{2}^\pm, \frac{3}{2}^\pm, (\frac{5}{2}^+)$		$\frac{1}{2}^\pm, \frac{3}{2}^\pm$	$E2$ to $\frac{1}{2}^+$, $M1$ to $\frac{3}{2}^+$	+
540.676(2)	$\frac{5}{2}^+$	540	2	$\frac{5}{2}^+$	$\frac{1}{2}^\pm, \frac{3}{2}^\pm, \frac{5}{2}^+$		$\frac{5}{2}^+$	$M1$'s to $\frac{3}{2}^+$'s	+
		596 [f]	4	$\frac{7}{2}^+(\frac{9}{2}^+)$					
604.513(3) [h]	$\frac{5}{2}^-$						$\frac{5}{2}^-$	$M1$'s to $\frac{5}{2}^-$ and $\frac{7}{2}^-(\frac{5}{2}^-)$	−
623.482(2)	$\frac{3}{2}^+$	623	0	$\frac{1}{2}^+$	$\frac{1}{2}^\pm, \frac{3}{2}^\pm, \frac{5}{2}^\pm$	$\frac{3}{2}^\pm, \frac{5}{2}^\pm$	$\frac{1}{2}^\pm, \frac{3}{2}^\pm$	$M1$ to $\frac{3}{2}^+$	+
645.9(5)	$\frac{7}{2}^-(\frac{5}{2}^-)$	644	4	$\frac{7}{2}^+$	$\frac{1}{2}^\pm, \frac{3}{2}^\pm, \frac{5}{2}^\pm, \frac{7}{2}^-$		$(\frac{5}{2}^-) \geq\frac{7}{2}$		
673.491(3)	$\frac{3}{2}^-$	671	1	$(\frac{3}{2}^-, \frac{1}{2}^-)$	$\frac{1}{2}^\pm, \frac{3}{2}^\pm$		$\frac{1}{2}^\pm, \frac{3}{2}^\pm, (\frac{5}{2}^+)$	$M1$ to $\frac{5}{2}^-$, $E2$ to $\frac{7}{2}^-(\frac{5}{2}^-)$	−
		712 [f]	(4)	$\frac{7}{2}^+(\frac{9}{2}^+)$					
722.043(3)	$\frac{1}{2}^+, \frac{3}{2}^\pm$	719 [g]	2	$(\frac{3}{2}^+)$	$\frac{1}{2}^\pm, \frac{3}{2}^\pm$		$\frac{1}{2}^\pm, \frac{3}{2}^\pm, \frac{5}{2}^+$	Feeds $\frac{5}{2}^+$	
		729 [f]	2	$\frac{5}{2}^+$					
Does not exist or $J=\frac{5}{2}^-, \geq\frac{7}{2}$		742 [g]	0	$\frac{1}{2}^+$					

TABLE VIII. *(Continued)*.

Present work E_{ex} (keV) [a] (adopted)	J^π [b] (adopted)	Previous work [c] E_{ex} (keV)	l	J^π	J^π limitations From primary transitions (Tables III, IV)	From angular distribution data at 2.96 eV (Table III)	From average Res. Capt. (Table VII)	From secondary transitions [d] and $(n,\gamma ce)$ multipolarities (Tables V and VI) transition	Parity
791.426(5)	$\frac{5}{2}^+$	789	2	$\frac{3}{2}^+,(\frac{5}{2}^+)$	$\frac{1}{2}^\pm,\frac{3}{2}^\pm,\frac{5}{2}^\pm$	$\frac{5}{2}^\pm$	$\frac{1}{2}^\pm,\frac{3}{2}^\pm,\frac{5}{2}^+$		
810.595(4)	$\frac{1}{2}^\pm,\frac{3}{2}^\pm$	809	2	$\frac{5}{2}^+$			$\frac{1}{2}^\pm,\frac{3}{2}^\pm$	Feeds $\frac{3}{2}^+$'s	
846.1(5)	$\frac{5}{2}^+$	843	2	$\frac{3}{2}^+$	$\frac{1}{2}^\pm,\frac{3}{2}^\pm,\frac{5}{2}^\pm,\frac{7}{2}^-$		$\frac{5}{2}^+$		
		883 [f]	5	$\frac{11}{2}^-$					
911.303(22)	$\frac{5}{2}^\pm$	909	2	$\frac{5}{2}^+$	$\frac{1}{2}^\pm,\frac{3}{2}^\pm,\frac{5}{2}^\pm$	$\frac{5}{2}^\pm$	$\frac{5}{2}^\pm$		
941.100(3) [h]	$\frac{3}{2}^-$	940 [g]	1	$\frac{3}{2}^-$	$\frac{1}{2}^\pm,\frac{3}{2}^\pm$		$\frac{1}{2}^\pm,\frac{3}{2}^\pm$	$M1$ to $\frac{5}{2}^-$, feeds $\frac{7}{2}^-(\frac{5}{2}^-)$	–
944.967(6)	$\frac{3}{2}^\pm$	946 [f]	0	$\frac{1}{2}^+$	$\frac{1}{2}^\pm,\frac{3}{2}^\pm,\frac{5}{2}^\pm$	$\frac{3}{2}^\pm$	$\frac{1}{2}^\pm,\frac{3}{2}^\pm$		
954.163(8)	$\frac{1}{2}^\pm$	954 [g]	0	$\frac{1}{2}^+$	$\frac{1}{2}^\pm,\frac{3}{2}^\pm,\frac{5}{2}^\pm$	$\frac{1}{2}^\pm,\frac{5}{2}^\pm$	$\frac{1}{2}^\pm,\frac{3}{2}^\pm$	Feeds $\frac{1}{2}^+$	
Does not exist or $J^\pi=\frac{5}{2}^-$ or $\geq\frac{7}{2}$		960 [f]	(0)	$(\frac{1}{2}^+)$					
981.755(9)	$\frac{5}{2}^+$	982	2	$\frac{5}{2}^+$	$\frac{1}{2}^\pm,\frac{3}{2}^\pm(\frac{5}{2}^+)$	$\frac{5}{2}^\pm$	$\frac{5}{2}^\pm$		
		1006 [g]							
1053.628(20)	$\frac{3}{2}^\pm$	1053	2	$(\frac{3}{2}^+)$	$\frac{1}{2}^\pm,\frac{3}{2}^\pm$	$\frac{5}{2}^\pm(\frac{3}{2}^\pm)$	$\frac{1}{2}^\pm,\frac{3}{2}^\pm$		
1065.8(5)	$\frac{1}{2}^\pm,\frac{3}{2}^\pm$	1065 [f]	0	$\frac{1}{2}^+$			$\frac{1}{2}^\pm,\frac{3}{2}^\pm$		
1091.0(5)	$\frac{5}{2}^+$	1092	2	$\frac{3}{2}^+,\frac{5}{2}^+$	$\frac{1}{2}^\pm,\frac{3}{2}^\pm,\frac{5}{2}^\pm$	$\frac{5}{2}^\pm$	$\frac{5}{2}^+$		
1111.8(5)	$\frac{1}{2}^\pm,\frac{3}{2}^\pm$				$\frac{1}{2}^\pm,\frac{3}{2}^\pm,(\frac{5}{2}^+)$		$\frac{1}{2}^\pm,\frac{3}{2}^\pm$		
1134.696(6)	$\frac{1}{2}^-,\frac{3}{2}^\pm$				$\frac{1}{2}^\pm,\frac{3}{2}^\pm$		$\frac{1}{2}^\pm,\frac{3}{2}^\pm$	Feeds $\frac{5}{2}^-$	
1147.7(5)	$\frac{1}{2}^\pm,\frac{3}{2}^\pm$	1146	2	$\frac{3}{2}^+$	$\frac{1}{2}^\pm,\frac{3}{2}^\pm$		$\frac{1}{2}^\pm,\frac{3}{2}^\pm$		
		1176 [g]	3	$(\frac{7}{2}^-)$					
1232.795(50)	$\frac{1}{2}^\pm,\frac{3}{2}^\pm$	1233	0	$\frac{1}{2}^+$	$\frac{1}{2}^\pm,\frac{3}{2}^\pm$		$\frac{1}{2}^\pm,\frac{3}{2}^\pm,\frac{5}{2}^+$		
1243.9(5)	$\frac{1}{2}^\pm,\frac{3}{2}^\pm$	1241 [g]	3	$(\frac{7}{2}^-)$	$\frac{1}{2}^\pm,\frac{3}{2}^\pm$		$\frac{1}{2}^\pm,\frac{3}{2}^\pm$		
1269.5(5)	$\frac{1}{2}^\pm,\frac{3}{2}^\pm,\frac{5}{2}^+$	1266	2	$\frac{5}{2}^+,(\frac{3}{2}^+)$	$\frac{1}{2}^\pm,\frac{3}{2}^\pm,\frac{5}{2}^+$		$\frac{1}{2}^\pm,\frac{3}{2}^\pm,\frac{5}{2}^+$		
		1308 [g]							
1328.4(5)	$\frac{5}{2}^\pm(\frac{3}{2}^\pm)$	1329 [g]	(1)	$(\frac{3}{2}^-)$	$\frac{1}{2}^\pm,\frac{3}{2}^\pm,\frac{5}{2}^\pm$	$(\frac{3}{2}^\pm)$	$\frac{5}{2}^\pm$		
1347.7(5)	$\frac{1}{2}^\pm,\frac{3}{2}^\pm,\frac{5}{2}^+$	1345	0	$\frac{1}{2}^+$			$\frac{1}{2}^\pm,\frac{3}{2}^\pm,\frac{5}{2}^+$		
1359.413(14)	$\frac{1}{2}^-,\frac{3}{2}^\pm$				$\frac{1}{2}^-,\frac{3}{2}^-(\frac{1}{2}^+,\frac{3}{2}^+)$		$\frac{1}{2}^\pm,\frac{3}{2}^\pm$	Feeds $\frac{5}{2}^-$'s	
1371.1(5)	$\frac{5}{2}^\pm$	1371 [f]	2	$\frac{5}{2}^+$	$\frac{1}{2}^\pm,\frac{3}{2}^\pm,\frac{5}{2}^\pm$	$\frac{5}{2}^\pm$	$\geq\frac{5}{2}^\pm$		
1378.1(5)	$\frac{1}{2}^\pm,\frac{3}{2}^\pm$				$\frac{1}{2}^\pm,\frac{3}{2}^\pm$		$\frac{1}{2}^\pm,\frac{3}{2}^\pm$		

TABLE VIII. *(Continued)*

Present work E_{ex} (keV) [a] (adopted)	J^{π} [b] (adopted)	Previous work [c] E_{ex} (keV)	l	J^{π}	J^{π} limitations: From primary transitions (Tables III, IV)	From angular distribution data at 2.96 eV (Table III)	From average Res. Capt. (Table VII)	From secondary transitions [d] and $(n,\gamma ce)$ multipolarities (Tables V and VI) transition	Parity
1399.0(5)	$\frac{1}{2}^{\pm},\frac{3}{2}^{\pm}$				$\frac{1}{2}^{\pm},\frac{3}{2}^{\pm}$		$\frac{1}{2}^{\pm},\frac{3}{2}^{\pm}$		
		1448 [f]	2	$(\frac{3}{2}^{+},\frac{5}{2}^{+})$					
1478.7(5) [i]	$\frac{1}{2}^{\pm},\frac{3}{2}^{\pm}$	1476	0	$\frac{1}{2}^{+}$	$\frac{1}{2}^{\pm},\frac{3}{2}^{\pm}$				
1484.9(5)	$\frac{1}{2}^{\pm},\frac{3}{2}^{\pm}(\frac{5}{2}^{+})$	1484 [g]	2(1)	$\frac{3}{2}^{+}(\frac{5}{2}^{-})$	$\frac{1}{2}^{\pm},\frac{3}{2}^{\pm}(\frac{5}{2}^{+})$				
		1499 [g]							
1537.3(5)	$\frac{1}{2}^{\pm},\frac{3}{2}^{\pm}$	1539 [f]	0	$\frac{1}{2}^{+}$	$\frac{1}{2}^{\pm},\frac{3}{2}^{\pm}$				
1540.3(5)	$\frac{3}{2}^{\pm}$	1541 [g]	(3)(2)	$(\frac{7}{2}^{-})(\frac{3}{2}^{+})$	$\frac{1}{2}^{\pm},\frac{3}{2}^{\pm},\frac{5}{2}^{\pm}$	$\frac{3}{2}^{\pm}$			
		1561 [g]							
1601.7(5)	$\frac{1}{2}^{\pm},\frac{3}{2}^{\pm}$	1600 [f]	(0)	$(\frac{1}{2}^{+})$	$\frac{1}{2}^{\pm},\frac{3}{2}^{\pm}$				
1615.8(5)	$\frac{1}{2}^{\pm},\frac{3}{2}^{\pm}$				$\frac{1}{2}^{\pm},\frac{3}{2}^{\pm}$				
1623.9(5)	$\frac{1}{2}^{\pm},\frac{3}{2}^{\pm},\frac{5}{2}^{\pm}$				$\frac{1}{2}^{\pm},\frac{3}{2}^{\pm},\frac{5}{2}^{\pm}$				
1644.6(5)	$\frac{1}{2}^{\pm},\frac{3}{2}^{\pm}$	1644	(2)	$(\frac{3}{2}^{+},\frac{5}{2}^{+})$	$\frac{1}{2}^{\pm},\frac{3}{2}^{\pm}$				
1647.8(5)	$\frac{1}{2}^{\pm},\frac{3}{2}^{\pm},\frac{5}{2}^{\pm}$				$\frac{1}{2}^{\pm},\frac{3}{2}^{\pm},\frac{5}{2}^{\pm}$				
		1656 [f]	(0)	$\frac{1}{2}^{+}$					
		1664 [g]	2(1)	$(\frac{3}{2}^{+})(\frac{3}{2}^{-})$					
1683.5(5)	$\frac{1}{2}^{\pm},\frac{3}{2}^{\pm}$	1682 [g]	0	$\frac{1}{2}^{+}$	$\frac{1}{2}^{\pm},\frac{3}{2}^{\pm}$				
		1692 [f]	0	$\frac{1}{2}^{+}$					
1710.2(5)	$\frac{1}{2}^{\pm},\frac{3}{2}^{\pm}$				$\frac{1}{2}^{\pm},\frac{3}{2}^{\pm}$				

[a] Uncertainties are denoted in parentheses and are on the last digit(s) of the corresponding entry. Excitation energies given to nearest tenth of keV are weighted averages of the thermal, resonance, and average capture primary γ-ray measurements; otherwise excitation energies are based on Ritz combinations of the curved crystal data.

[b] See explanatory notes in text. J^{π} is obtainable by combining the information given in columns 6–10. Note that columns 6–8 are complete (they summarize all the relevant data) whereas column 9 only gives the information from the secondary transitions actually needed to define the level spin.

[c] From Table I in Ref. 2. E_{ex} values listed here are the averages of those given in Ref. 2. Note that the measurements of Refs. 1 and 2 consisted of the quoted l values in the (d,p) and (d,t) reactions. The specific assigned J^{π} values involved additional shell model arguments.

[d] The notation $M1$ to $\frac{5}{2}^{+}$ means that the level in question deexcites by an $M1$ transition to a $\frac{5}{2}^{+}$ level; $M1$'s to $\frac{1}{2}^{+}$ and $\frac{5}{2}^{+}$ denotes two different $M1$ deexcitation γ rays; $M1$ to $\frac{7}{2}^{-}(\frac{5}{2}^{-})$ denotes a transition to a state whose spin is limited to $\frac{7}{2}^{-}(\frac{5}{2}^{-})$; "feeds" or "fed from" means that the transition multipolarity could not be determined from the $(n,\gamma ce)$ data and therefore that the limitation on J^{π} from this transition is based on an assumed multipolarity of $E1$, $M1$, or $E2$.

[e] Level spin taken from literature (Ref. 15). Present data are consistent with this J^{π}.

[f] Level populated only in the (d,t) reaction.

[g] Level populated only in the (d,p) reaction.

[i] 1478.7 keV level may be a doublet.

[h] See text for detailed discussion of 604 and 941 keV levels.

to be questionable placements in the level scheme. Consequently, the uncertainty for the excitation energy is taken to be the larger of the two γ-ray energy uncertainties. It is possible, however, that neither placement is correct, in which case an energy and uncertainty of 1233.5 ± 0.5 keV come from the primary transition alone.

1359.413(14) keV; $\frac{1}{2}^-, \frac{3}{2}^\pm$. This level is populated in the thermal reaction by the most intense primary γ ray, as well as in the 2.96 eV resonance. Therefore, J^π must be $\frac{1}{2}^\pm$, $\frac{3}{2}^\pm$ and is most likely to be negative parity. The γ ray to the 339 keV level $(\frac{5}{2}^-)$ rules out $\frac{1}{2}^+$ for the 1359 keV state. The 418.298(7) keV γ ray could be placed between the 1359 and 941 keV levels, based upon energy combination. However, the intensity ratio for this γ ray is 0.5, and such a placement is, therefore, inconsistent with the population of this state.

Since the 1359 keV state is populated by the most intense thermal primary transition and since it decays predominantly to negative-parity states, it is of interest to place limits on the possibility of decay to other states below 339 keV (i.e., by γ rays beyond the energy cutoff of the curved crystal data). Inspection of the Ge(Li) detector spectrum for thermal capture for the energy range of 1.0 to 1.4 MeV revealed that there are peaks at 1032.5, 1034.1, and 1114.3 keV which could be transitions between the 1359 keV state and levels at 326, 325, and 245 keV, respectively. (There is no evidence of a 1359.4 keV transition to the ground state.) However, for each of these, the peak in the resonance data is nearly the same intensity, thereby ruling out an origin in the 1359 keV level whose population in thermal capture is 7.8 times as large as in the 2.96 eV resonance.

By virtue of the strong population by a thermal capture primary transition, the 1359 keV level leads to considerable population of a negative-parity system of levels at lower energy. Since such a strong primary intensity is statistically unlikely such families are seldom observed, especially in the complete fashion obtained here. These data therefore provide an unusual but long sought for opportunity to study the low-spin states of unique parity that have the same parentage as the high-spin yrast levels that are of high current interest.

D. Spectroscopic factors

Table VIII compares the present results with the earlier (d,p) and (d,t) results.[1,2] The transfer reactions, of course, are sensitive primarily to the orbital angular momentum transfer and not to the final state spin. However, from a shell model dependent analysis of the ratios of (d,p) and (d,t) spectroscopic factors, the authors of Refs. 1 and 2 interpreted their data to provide tentative J values for many levels. Comparison of the two sets of J^π assignments shows a number of cases of agreement, a number of cases where one of the currently allowed values of J^π agrees with the earlier assignment, and several levels where definite discrepancies exist. Most of the previously assigned $J^\pi = \frac{7}{2}^+$ states are included in this last category.

Table IX lists the previous spectroscopic factors and those currently reevaluated for levels whose J values are redefined in the present work. The table does not include the 1243 keV level since too many possibilities still exist. The new spectroscopic factors were obtained from the data of Refs. 1 and 2 combined with the currently revised J^π

TABLE IX. Spectroscopic factors for some levels in ^{109}Pd.[a]

E_{ex} (keV)	Previous[b] J^π	$S(d,p)$	$S(d,t)$	Current J^π	$S(d,p)$	$S(d,t)$
245.1	$\frac{7}{2}^+$	0.44	2.3	$\frac{7}{2}^-(\frac{5}{2}^-)$	0.08	~0.4
426.1	$\frac{7}{2}^+$	0.20	4.0	$\frac{7}{2}^+$	≤0.20[c]	≤4.0[c]
433.6				$\frac{3}{2}^+$	≤0.038[c]	≤0.304[c]
623.5	$\frac{1}{2}^+$	0.053	0.056	$\frac{3}{2}^+$	0.095	0.162
645.9	$\frac{7}{2}^+$	0.12	0.46	$\frac{7}{2}^-(\frac{5}{2}^-)$	0.02	~0.01
791.4	$\frac{3}{2}^+$	0.053	...	$\frac{5}{2}^+$	0.031	0.179
	$(\frac{5}{2}^+)$	...	0.179			
810.6	$\frac{5}{2}^+$	0.022	0.27	$\frac{1}{2}^{(+)}$	0.022	0.13
				$\frac{3}{2}^{(+)}$	0.038	0.35
846.1	$\frac{3}{2}^+$	0.062	0.10	$\frac{5}{2}^+$	0.036	0.08
945.0	$\frac{1}{2}^+$	...	0.034	$\frac{3}{2}^{(+)}$	...	~0.1
1091.0	$\frac{3}{2}^+$	0.016	...			
	$\frac{5}{2}^+$	...	0.079	$\frac{5}{2}^+$	0.009	0.079

[a] Entries are given for levels where the J^π value assigned in earlier (d,p) or (d,t) work (Refs. 1 and 2) are updated by the newly determined value(s). Where the parity of a level is uncertain we have taken it as positive for the purposes of this table and placed parentheses around the parity symbol.

[b] Taken from Refs. 1 and 2. Note that both the 791.4 and 1091.0 keV levels are assigned there as $\frac{5}{2}^+$ from (d,t) and $\frac{3}{2}^+$ from (d,p). We obtain $J=\frac{5}{2}$ for both levels, and thus the (d,p) but not the (d,t) spectroscopic factors are changed.

[c] The upper limits quoted refer to the unresolved question of whether one or both levels are populated in the charged particle reactions. It seems probable from the measured excitation energies, however, that most of the cross section is to the 426 keV $\frac{7}{2}^+$ level in which case the entries for that level can be read without the ≤ symbols.

values. One notes from Table IX that significant changes in the S factors arise, particularly for the previously assigned $\frac{7}{2}^+$ states. These changes occur because the DWBA cross sections decrease rapidly as l and j grow larger and, thus, the same experimental cross section generally represents a larger spectroscopic factor if the state is a higher spin state than if it is assigned a lower spin. Thus, one consequence of the new spin assignments is the revision of the corresponding spectroscopic factors and, in effect, the consequent removal of large amounts of $g_{7/2}$ spectroscopic strength without significantly changing the spectroscopic strengths for other shell model orbits. The effect of the revised spin assignments on the degree of orbital filling is discussed in Sec. III.

E. Statistical behavior of primary transition intensities

It is interesting to use the more reliable set of spin assignments now available for ^{109}Pd to determine if the intensity distribution of primary γ-ray transitions may contain information on the neutron capture mechanism itself.

For most nuclei the primary transition strengths (partial radiative widths) follow a statistical distribution which has been successfully interpreted in terms of the hypothesis of the formation and decay of a complex compound nuclear capture state. However, in certain mass regions the centroids of the $2p$, $3p$, and $3s$ shell model orbits lie near the neutron binding energy; that is, the neutron strength functions for these orbits attain their maximum values. In these regions one may expect the capture state to contain larger than statistically expected components of the relevant single particle state. Transitions to certain other low-lying single particle states might then be expected to be relatively enhanced, leading to deviations from a purely statistical spectrum of primary γ-ray intensities. These qualitative ideas have received formal expression in the valence neutron model.[29-36] which has had quantitative success[13,32-36] in predicting partial radiative $E1$ widths following neutron capture in ^{24}Mg, ^{36}Ar, ^{50}Cr, ^{54}Fe, ^{58}Ni, $^{90-98}$Zr, and ^{92,98}Mo, nuclei which in fact lie in the above mentioned regions of strength function maxima.

For ^{108}Pd the $3p$ strength function has decreased by a factor of ~2 from its maximum value of $S1 = 7.0 \times 10^{-4}$ attained in ^{96}Zr and ^{98}Mo and, therefore, this nucleus provides an interesting test case for the model.

The discussion that follows uses the absolute primary transition strengths given in Table III to deduce partial radiative widths $\Gamma_{\gamma if}$ for ^{109}Pd after application of a correction for the angular anisotropy of the γ rays. It also assumes that levels not assigned negative parity are in fact positive parity. Using the experimental angle-averaged intensities $\langle I_{if} \rangle$, the partial radiative widths $\Gamma_{\gamma if}$ were extracted using the total radiative width Γ_γ for the 2.96 eV resonance given in BNL 325.[19] If we consider positive-parity low-lying levels of ^{109}Pd, these empirical widths refer to $E1$ multipolarity following p-wave capture.

The $\Gamma_{\gamma if}$ can be compared with the valence neutron model (VN) predictions obtained from the expression (see Ref. 30, p. 327 and Ref. 33)

$$(\Gamma_{\gamma if})_{\mathrm{VN}} = \frac{16\pi k^3}{9}\,\theta_i^2\theta_f^2 \left| \bar{e} \int_0^\infty dr u_i r u_f \right|^2 \times \frac{|\langle jIJ_i || Y^{(1)} || j'IJ_f \rangle|^2}{2J_i + 1}, \tag{1}$$

where k is the photon wave number, θ_i^2 and θ_f^2 are initial and final state reduced widths, $\bar{e}$ is the effective charge given by $-eZ/A$, and u_i and u_f are the initial and final single particle radial wave functions. In the geometrical factor, J_i and J_f are the spins of the initial ($\frac{3}{2}$) and final levels, I is the spin of the core, which is zero for an even-even target nucleus, and j and j' are the single particle angular momenta which for $I=0$ are equal to J_i and J_f, respectively.

The essential physics on the model is contained in the reduced widths θ_i^2 and θ_f^2, which depend on the l and j of the shell model orbit, and which are related to the single particle structure of the initial and final states. Thus, $\theta_f^2 = S(d,p)$ and, therefore, the calculated $(\Gamma_{\gamma if})_{\mathrm{VN}}$ are proportional to the (d,p) spectroscopic factors and, therefore, to the measured (d,p) cross sections. One must note, however, that the valence model describes only one amplitude in the radiative neutron capture mechanism. This component may be expected to dominate (e.g., over compound nuclear formation) only for those low-lying states with large spectroscopic factors. For other levels one must expect the correlation of the measured and valence model widths to be masked by strong statistically varying contributions to the total $\Gamma_{\gamma if}$.

The quantity θ_i^2 is given by γ_n^2/γ_{sp}^2, where γ_n^2 is the reduced neutron width of the capture state and γ_{sp}^2 is the single particle reduced width. In Lynn's prescription,[30] γ_{sp}^2 is taken to be the value for a square well potential. Since the two corrections to this prescription pointed out by Lane and Mughahghab[31] approximately cancel we have taken Lynn's values[30] for both γ_{sp}^2 and for the radial integrals in accordance with continuing custom.[36]

The qualitative result of the calculations is that the $(\Gamma_{\gamma if})_{\mathrm{VN}}$ for $p_{3/2} \rightarrow d_{3/2}$ transitions are lower by a factor of ~10 compared to $p_{3/2} \rightarrow s_{1/2}$ or $p_{3/2}$

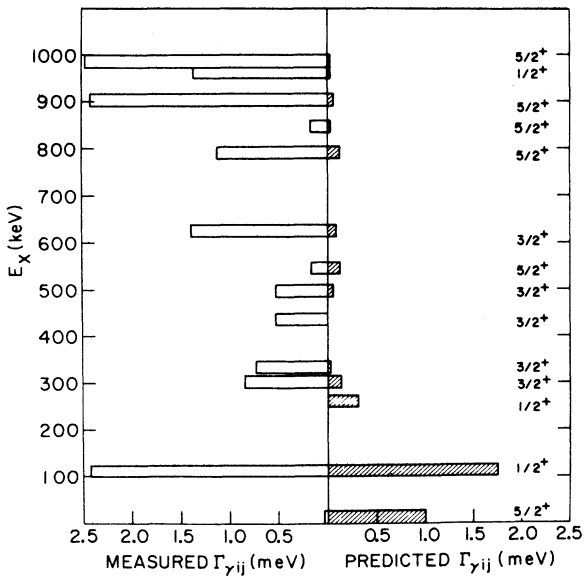

FIG. 9. Comparison of the measured partial radiative widths for the 2.96 eV resonance with those predicted from empirical (d,p) spectroscopic factors according to the formalism of the valence capture model. The labels on the right denote the J^π values used for each state. The J^π values and spectroscopic factors used are taken from the results of Refs. 1 and 2 except where these have been corrected in the present work.

$\rightarrow d_{5/2}$ transitions for states with the same $S(d,p)$. Thus, low-lying $s_{1/2}$ levels with large spectroscopic factors should be populated by intense primary transitions while those to low-lying $d_{3/2}$ states are predicted to be much weaker.

A quantitative comparison of measured $\Gamma_{\gamma if}$ and those predicted by the model is given in Fig. 9. As is evident, the model calculation for the dominant $p_{3/2} \rightarrow s_{1/2}$ transition to the 113 keV level is in agreement with the data. The higher-lying $d_{3/2}$ and $d_{5/2}$ states generally have smaller $S(d,p)$ values so that more complex reaction mechanisms mask any valence contribution and the comparison provides little information. For the $d_{5/2}$ ground state, the discrepancy apparent in Fig. 9 is striking and represents a clear disagreement with the model although, admittedly, the $S(d,p)$ value for the ground state is only ~0.18. This is considerably lower than in the lighter Zr and Mo isotopes, where the valence neutron model is successful.

III. DISCUSSION

A. Filling of the $g_{7/2}$ and $h_{11/2}$ orbits

Table X presents the old and new spectroscopic factors for the (d,p) and (d,t) reactions into ^{109}Pd summed over all states studied in Refs. 1 and 2. The current values include the deletion of the $l=0$ strength from the 382, 404, 742, and 960 keV levels now thought either not to exist or to have $J \geq \frac{5}{2}$ on the basis of their nonobservance in average capture. As expected from the results and discussion of Table IX, the $S(\frac{7}{2}^+)$ entries are the most significantly affected by the current results.

Table XI shows the systematics of the summed spectroscopic factors for several nuclei in this region, for the uniform excitation energy range 0–920 keV. The upper energy cutoff is determined by the limited (d,t) data[37] available for ^{103}Ru. In parentheses below some of the entries, however, are the spectroscopic factor sums that would be obtained for a fuller energy range where this can be evaluated. Such entries are made only when the extended sum differs by 15% or more from the values tabulated for 0–920 keV.

The systematics evident in the table are revealing. Rather consistent numbers are obtained for a given reaction for the $s_{1/2}$, the combined $d_{3/2}$, $d_{5/2}$ orbitals, and for the $h_{11/2}$ orbital. [Note that since both the $d_{3/2}$ and $d_{5/2}$ orbits are being actively filled in this region, the empirical distinction between the two spins, which relied in Ref. 1 and 2 not on the l transfer but on the ratio $S(d,t)/S(d,p)$, is more ambiguous than for other orbits and it is, therefore, safest to consider the combined S factor sums for both spins.] For the $g_{7/2}$ orbit, the current revised results for ^{109}Pd bring these quantities into reasonable consistency with the data for ^{103,105}Ru. Furthermore, the $\Sigma S(d,p)$ value for ^{109}Pd is now much closer to that for the neighboring Sn isotopes (see Table I), which suggests that a major source of the apparent $g_{7/2}$ anomaly was misassigned spin values for the 245 and 646 keV levels.

A meaningful way to investigate further the experimental trends is in terms of the equivalent number of neutrons in each orbit. This quantity is related to the spectroscopic factors via

TABLE X. ^{109}Pd: Summed spectroscopic factors.

	$\Sigma S_j(d,p)$		$\Sigma S_j(d,t)$	
Orbit	Previous[a]	Current[b]	Previous[a]	Current[b]
$\frac{1}{2}^+$	0.52	0.46	1.14	1.00
$\frac{3}{2}^+$	0.86	0.87[c]	1.45	1.96[c]
$\frac{5}{2}^+$	0.24	0.30	2.70	2.51
$\frac{7}{2}^+$	0.76	≤0.20	7.36	≤4.6

[a] Taken from data tables of Refs. 1 and 2.

[b] Taken from Refs. 1 and the substitutions given in Table IX.

[c] The values listed assume no contribution from the 433.6 keV level and that the 810.6 keV level is $\frac{3}{2}^+$.

TABLE XI. Summed spectroscopic factors and number of neutrons for different j-shells for several $A \sim 100$ nuclei. $E_{ex} = 0-920$ keV. Numbers in parentheses are the spectroscopic factor sums obtained for wider excitation energy ranges, as available; namely, up to 2.5 MeV for ^{109}Pd, 1.3 MeV for ^{107}Pd, and 1.9 MeV for the (d,p) entries for ^{103,105}Ru. These numbers are a guide to the effect of truncating the energy range and are given only if they differ from the principal entry by more than 15%. Values for N_j are obtained using Eqs. 2 and 3.

Orbit		(d,p) ^{103}Ru[a]	(d,p) ^{105}Ru[a]	(d,p) ^{107}Pd[b]	(d,p) ^{109}Pd[c]	(d,t) ^{103}Ru[b]	(d,t) ^{107}Pd[b]	(d,t) ^{109}Pd[c]
$\frac{1}{2}^+$	ΣS_j	0.51	0.57	0.51	0.37 (0.46)	0.78	0.63	0.59 (1.00)
	N_j	0.98	0.86	0.98	1.3	0.78	0.63	0.59
$\frac{3}{2}^+$, $\frac{5}{2}^+$	ΣS_j[d]	0.63[e] (0.77)	0.64[e] (0.80)	0.76 (0.90)	0.93[f] (1.17)[f]	3.63	3.43	3.57[f] (4.46)[f]
	N_j	6.3[e]	6.2[e]	6.4[g]	5.7[g]	3.63	3.43	3.57[f]
$\frac{7}{2}^+$	ΣS_j	0.42	0.23	0.71	≤ 0.20	2.83	4.60	≤ 4.6
	N_j	4.64	6.16	2.32	≥ 6.4	2.83	4.60	≤ 4.6
$\frac{11}{2}^-$	ΣS_j	0.27	0.28	0.29	0.28	1.92	1.67	2.91
	N_j	8.8	8.6	8.5	8.6	1.92	1.67	2.91
ΣN_j $j \neq \frac{11}{2}$		11.9	13.1	9.7	≥ 13.5	7.2	8.7	≤ 8.7

[a] From Refs. 37 and 38. The excitation energies of Ref. 37 are in error because of a missed ground state for ^{105}Ru. Reference 38 also leads to slightly different $S(d,p)$ values for ^{105}Ru.

[b] From Refs. 1 and 2.

[c] From Refs. 1 and 2 and present work.

[d] The empirical distinction between spin assignments of $\frac{3}{2}^+$ and $\frac{5}{2}^+$ is somewhat uncertain for these two actively filling orbits. Thus, we prefer to tabulate the combined spectroscopic sums for these orbits.

[e] $\Sigma S(d,p)$ and $N_j(d,p)$ values for ^{103,105}Ru are obtained assuming all $l=2$ transitions populate $\frac{5}{2}^+$ states. The $N_j(d,p)$ values will differ slightly if some of the $l=2$ transitions populate $\frac{3}{2}^+$ states due to slightly different $\sigma_{DW}(\frac{5}{2}^+)$ and $\sigma_{DW}(\frac{3}{2}^+)$ cross sections.

[f] Assumes no contribution from the 433.6 keV level and that the 810.6 keV level is $\frac{3}{2}^+$.

[g] To calculate $N_j(d,p)$ the following values for $\Sigma S_j(d,p)$ ($E_{ex} \leq 920$ keV) for $\frac{3}{2}^+$ and $\frac{5}{2}^+$ orbits were used: $\Sigma S_{3/2}(d,p) = 0.47$ and 0.64, $\Sigma S_{5/2}(d,p) = 0.29$ and 0.29 for ^{107,109}Pd, respectively.

$$N_j(d,p) = (2j+1)[1 - \Sigma S_j(d,p)]$$

and (2)

$$N_j(d,t) = \Sigma S_j(d,t),$$

where N_j is the number of neutrons in the orbit of spin j as determined from the (d,p) or (d,t) reaction data. The N_j's deduced from Table X are presented in Table XI. In order to relate $N_j(d,p)$ to $N_j(d,t)$, recall the definition of the S factors in terms of the usual orbital occupation parameters U^2 and V^2:

$$\Sigma S_j(d,p) = U_j^2 = 1 - V_j^2$$

and (3)

$$\Sigma S_j(d,t) = (2j+1)V_j^2 .$$

Substituting Eq. (3) into Eq. (2), one obtains the expected result $N_j(d,p) = N_j(d,t)$.

Formally this in incorrect, since $\Sigma S(d,p)$ is equal to U^2 for the target nucleus of the (d,p) reaction, of mass $A-1$, whereas, $\Sigma S(d,t)$ is related to V^2 for the (d,t) target of mass $A+1$. However, away from closed shells, this is a minor effect and one expects the equality in N values to hold approximately. Large empirical inequalities are therefore physically interesting.

If

$$N_j(d,p) > N_j(d,t)$$

it suggests that states of spin j have been missed since Eqs. (2) and (3) show that as more spin j states are found, $N_j(d,p)$ *decreases* and $N_j(d,t)$ *increases*. Of course, *small* inequalities are expected since one always investigates a finite range of excitation energies and there is the possibility of missing weak transitions.

Conversely, if

$$N_j(d,p) < N_j(d,t),$$

it suggests that some states have been incorrectly assigned spin j.

Table XI shows that the $N_j(d,p)$ and $N_j(d,t)$ values for $j=\frac{1}{2}$ are quite close to one another. For the rather high-lying $d_{3/2}$ orbit, it is certainly expected that not all the strength is identified and it is, therefore, not surprising that $N_{3/2}(d,p)+N_{5/2}(d,p) > N_{3/2}(d,t)+N_{5/2}(d,t)$. Furthermore, note that, from Eq. (2), for $\Sigma S_j(d,p)$ values near unity the uncertainties in the corresponding $N_j(d,p)$ values can be large. Nevertheless, for either (d,p) or (d,t) alone, the entries in Table XI vary only slightly from one nucleus to another.

For the $g_{7/2}$ orbit, $N_{7/2}$ for ^{109}Pd is in good agreement with the values for Ru. More importantly, $N_{7/2}(d,p) > N_{7/2}(d,t)$ for ^{103}Ru and ^{109}Pd. These results suggest a consistent and smooth pattern of $g_{7/2}$ orbit filling in this mass region as well as the not unexpected result that some $g_{7/2}$ strength remains to be found at higher excitation energies.

However, the $N_{7/2}$ values for ^{107}Pd are now unique in that $N_{7/2}(d,p)$ is *less than* $N_{7/2}(d,t)$. As shown above, this perhaps suggests a misassignment in ^{107}Pd; the most likely candidate is the 367 keV state whose previous $\frac{7}{2}^+$ assignment relies partly on an $l=4$ (d,t) transition with uncharacteristic angular distribution. The removal of the $\frac{7}{2}^+$ assignment for the 367 keV level would change the $S(d,p)$ and $S(d,t)$ entries for ^{107}Pd in Table XI to 0.26 and 2.78, respectively, bringing these numbers [and corresponding $N_{7/2}$ values) into consistency with the results for other neighboring nuclei (see Tables X and XI)]. On the other hand, if the $\frac{7}{2}^+$ assignments in ^{107}Pd are correct, this nucleus now would be the *only* one in this region[37-44] (comprising ^{103,105}Ru, ^{101,103,105,107,109}Pd, ^{115}Cd, ^{111,113,115,117,119,121,123}Sn) that would have two strongly populated low-lying $\frac{7}{2}^+$ states. The firm determination of level spins in ^{107}Pd must now be considered a matter of renewed interest since fragmentation of the $l=4$ strength would suggest that new degrees of freedom, even at low excitation energies, are important in this region.

The original $g_{7/2}$-$h_{11/2}$ anomaly had two facets, the apparent emptiness of the $g_{7/2}$ orbit in the Pd region compared to the Sn nuclei and the apparently greater occupation of the $h_{11/2}$ than the $g_{7/2}$ orbit. The above discussion largely resolves the first point. The present data themselves shed no new light on the second, or $h_{11/2}$ part of the anomaly but the entries in Table XI do shed light. The essential point is that throughout this region $N_{11/2}(d,p) \gg N_{11/2}(d,t)$.

From the above discussion, this simply suggests that $\frac{11}{2}^-$ levels with significant single particle amplitudes exist at higher excitation energies than are probed by the existing (d,p) and (d,t) studies. The identification of such states would reduce $N_{11/2}(d,p)$ and increase $N_{11/2}(d,t)$. The fact that, for each reaction alone, the current values for $N_{11/2}$ are nearly constant for the nuclei of Table XI implies a similarity in structure of the lowest-lying $\frac{11}{2}^-$ state in each nucleus and perhaps a similar pattern of higher energy $\frac{11}{2}^-$ fragmentation. The calculations of Ref. 9 support the hypothesis of higher-lying $h_{11/2}$ strength in this region.

B. Negative- (unique-) parity states

The family of negative-parity levels between 189 and 1359 keV is of considerable importance. These levels are low lying (all but one below 1 MeV) and therefore cannot correspond to the coupling of positive-parity single particle states with negative parity (e.g., 3^- or 5^- states) of the even-even Pd core since the latter only occur above ~2 MeV. Similarly, they are too low in energy to contain significant amplitudes for the negative-parity single particle states from the $N=82-126$ shell. They must therefore be predominantly unique-parity levels constructed by coupling an $h_{11/2}$ neutron to the low-lying positive-parity excitations of the core. As such, they form an *isolated family, even though they have low spin.* Furthermore, they are therefore related to the high-spin unique-parity levels in the lighter Pd isotopes which form the yrast sequences observed in heavy-ion reactions, and which are intimately related to the nature and interpretation of backbending in adjacent even-even nuclei.

In the Nilsson model with Coriolis mixing, for the case of the Fermi surface near the low-K unique-parity orbits, the structure of such sequences of states is that of a decoupled particle combined with a core rotation whose angular momentum vector is generally parallel to that of the odd particle. This alignment results directly from the action of the Coriolis force and is therefore strongest for moderately deformed nuclei where the Coriolis coupling constant $\hbar^2/2\mathcal{I}$ is large. The result is the development of an approximate coupling scheme, called rotation aligned,[4] in which the rotational angular momentum (R) of the core is an approximate constant of the motion. This structure gives rise to rotational bands whose successive members differ by two units in the core rotation and whose spin sequence is therefore $\Delta J=2$ with energy spacings approximating those of the adjacent even-even core nucleus. Despite the apparent success and general acceptance of these ideas and their frequent use as a framework for the interpretation of high-spin states, one would like to have further tests of these concepts since the existing ones invariably center on the high-

spin states for which they were designed. As emphasized by Rekstad and coworkers,[10,45,46] such a test might fruitfully involve the low-spin, anti-aligned levels with the same parentage as the aligned high-spin states. As with the aligned states the low-spin levels may be either favored or unfavored. By favored is meant those levels of the $\vec{J}=\vec{j}\otimes\vec{R}$ coupling for which $J=|j\pm R|$, that is, states with maximum parallelism or antiparallelism of $\vec{j}$ and $\vec{R}$. The unfavored levels are all the other states of the $\vec{j}\otimes\vec{R}$ system. Note that an unfavored level of the same spin as a favored level requires a higher core angular momentum and, therefore, should occur at higher energy. Note also that some low-spin levels will have $R>j$. A test including these anti-aligned state is now possible with the negative-parity levels disclosed in ^{109}Pd. It is important to emphasize that these levels occur on the same footing in the Nilsson model as the high-spin levels. They have comparably high R values. For example, in the extreme weak coupling or rotation aligned pictures, both the $\frac{1}{2}^-$ and $\frac{23}{2}^-$ favored levels have $R=6$ and the favored $\frac{3}{2}^-$ and $\frac{19}{2}^-$ levels equally have $R=4$. Furthermore, being of *unique parity*, the low-spin states are just as isolated as the high-spin yrast levels and, in fact, perhaps even more so since in practice they lie somewhat lower in energy than the high-spin levels with the same R values and since there are fewer of them. For example, there are only two $\frac{3}{2}^-$ and one $\frac{1}{2}^-$ levels in the unique-parity basis as compared with six $\frac{23}{2}^-$ and six $\frac{19}{2}^-$ states.

The sequences of aligned and anti-aligned levels naturally fall into categories depending on the degree of parallelism. Furthermore, as shown by Løvhøiden and Rekstad,[10] each family has a roughly parabolic dependence of energy on spin. Rekstad *et al.*[45] have introduced a useful format, elegantly summarized in Ref. 46, for displaying these states by plotting their energies vs a projection of total spin $\vec{J}$ on $\vec{j}$ instead of along $\vec{R}$. This yields the symmetric parabolas shown in Fig. 10 where each is labeled by an index n relating to the

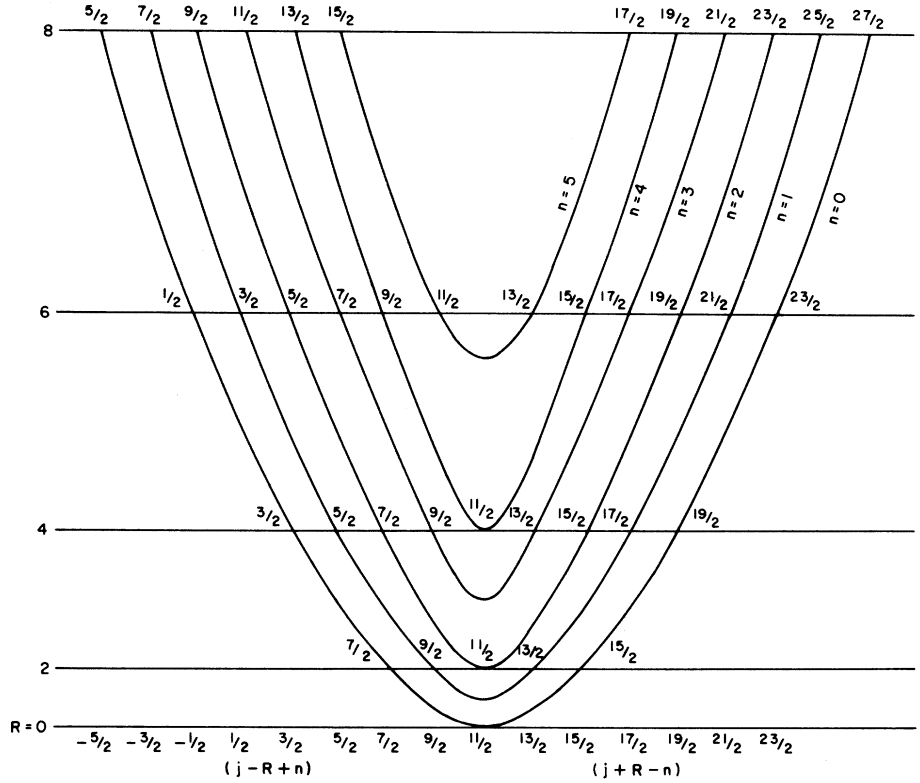

FIG. 10. States formed by an $h_{11/2}$ particle and a symmetric rotor core in the extreme weak coupling limit. All states with the same core rotational angular momentum ($\vec{R}$) are degenerate in energy. The abscissa is a projection of the total angular momentum ($\vec{J}$) onto the particle angular momentum ($\vec{j}$). Spins are explicitly noted at the intersection of the straight line denoting the core rotational energy $[\alpha R(R+1)]$ and each of the parabolas. For an $h_{11/2}$ particle there are six parabolas, each denoting a different degree of alignment between $\vec{R}$ and $\vec{j}$ ($n=0$ corresponds to maximum alignment).

angle between $\vec{R}$ and $\vec{j}$. [Figure 10 is constructed via a weak coupling picture with $R(R+1)$ core spacings in the limit of no coupling between particle and core. More realistic situations are discussed below.] The allowed states occur for intersections of the parabolas at half-integer abscissa values with the horizontal lines corresponding to the energies of core rotations. For aligned states, and for anti-aligned ones with $R<j$, the level spins are given by the abscissa value. The spin sequence along a parabola is $\Delta J=2$ except that, once on each parabola, when $\vec{R}$ is antiparallel to $\vec{j}$ and changes from $<j$ to $>j$, there is a jump of $\Delta J=1$. Thus, for anti-alignment and $R>j$ the level spin is not given by the abscissa value.

The unique-parity levels found in this study are extracted from the full level scheme and summarized in Fig. 11. In the context of the rotation aligned scheme as outlined above, the $\frac{11}{2}^-$, first $\frac{7}{2}^-$ first $\frac{3}{2}^-$, and $\frac{1}{2}^-$ levels form the $\Delta J=2$ (the $\frac{1}{2}$ level corresponds to the $\Delta J=1$ jump at $R>j$) favored anti-aligned sequence ($n=0$ parabola). The $\frac{9}{2}^-$, first $\frac{5}{2}^-$, and second $\frac{3}{2}^-$ levels belong to the $n=1$ parabola and the second $\frac{7}{2}^-$ and second $\frac{5}{2}^-$ levels are from the third ($n=2$) parabola. The levels with $J\leq\frac{5}{2}$ form the complete set of low-spin states expected for the odd particle in the $h_{11/2}$ orbit (except for an expected high-lying $\frac{5}{2}^-$ level with $R=8$). This is the first time that such a complete set of anti-aligned levels has been observed. Note particularly that three of the levels, the $\frac{1}{2}^-$, second $\frac{3}{2}^-$, and second $\frac{5}{2}^-$ states have $R>j$, the first time any such levels have been disclosed in medium or heavy mass nuclei.

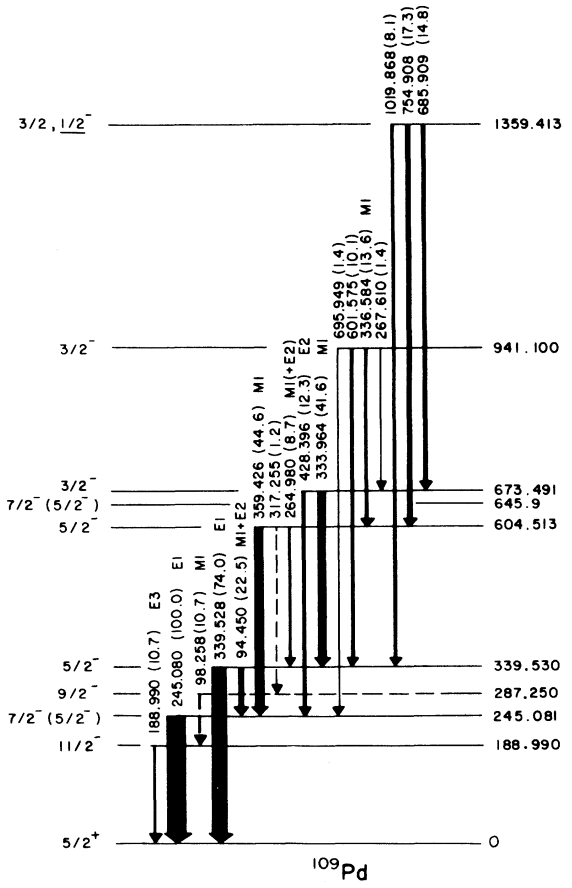

FIG. 11. Negative-parity levels observed in ^{109}Pd. Relative γ-ray intensities have been normalized so that $I_{245}\equiv 100$. The underlined J^π assignment for the 1359 keV state is the preferred value.

The fact that the full set of expected low-spin levels is found is indeed satisfying, but at the same time one immediately notes discrepancies with the simple model outlined above and in Fig. 10. First, one expects enhanced $E2$ cascade transitions along a parabola (these correspond to $\Delta R=2$ changes in core rotation) and $M1$ transitions between states with $\Delta J=\pm 1$ and the same R value. Transitions between parabolas which also change the R value should be very weak, and changes in R of more than two units should be forbidden for $E2$ transitions. Some of the observed transitions agree with these predictions, such as the 428 keV $E2$ transition from the lowest $\frac{3}{2}^-$ level at 673 keV to the $\frac{7}{2}^-$ state at 245 keV or the $\frac{3}{2}^-\rightarrow\frac{5}{2}^-$ $M1$ transitions of 336 and 333 keV. However, transitions such as the two $\Delta R=4$ (with change in n also) transitions [$941(\frac{3}{2}^-)\rightarrow 245(\frac{7}{2}^-)$ keV and $604(\frac{5}{2}^-)\rightarrow 245(\frac{7}{2}^-)$ keV] are surprising as is the strength of the $1359(\frac{1}{2}^-)\rightarrow 604(\frac{5}{2}^-)$ keV transition, which is $\Delta n=2$ with no change in R, and the strength of the $1359(\frac{1}{2}^-)\rightarrow 339(\frac{5}{2}^-)$ keV transitions with changes in both R and degree of alignment. Furthermore, it is immediately evident that the energy spacings are seriously at variance with the simple predictions of Fig. 10. For example, the three $R=6$ states (1359, 941, 604 keV) should have been degenerate. Also, while the $R=6$ to $R=4$ core spacing in ^{108}Pd is 700 keV which is reasonably close to the 1359–673 and 941–339 keV spacings, the 604–339 keV distance is quite different. Finally, the $R=4\rightarrow R=2$ spacings (673–245 keV and 339–287 keV) should have been equal. Clearly, then though all the required states appear to be present, their wave functions must be significantly perturbed relative to the pure $|JjR\rangle$ wave functions of Fig. 10.

In practice, of course, one is not limited to the extreme situation in Fig. 10. As noted above, that figure is effectively constructed from a weak coupling picture with $R(R+1)$ core spacings and in the limit of no coupling, whereas practical calculations of rotation-aligned-like spectra are usually performed in the basis of the Nilsson mod-

el with Coriolis coupling. Such Nilsson model calculations, in fact, have already been successfully applied by Smith and Rickey[9] to the high-spin aligned $h_{11/2}\otimes$rotor states observed[5-7] in ^{101,103,105}Pd. The calculations employed the usual Nilsson model with a deformation of $\delta=0.12$ and a modified VMI[47] prescription to simulate nonrotor anharmonicities in the core spacings. These Coriolis calculations utilized a constant matrix element attentuation factor of $\alpha=0.8$. The excellent agreement obtained for ^{105}Pd (the isotope with the largest number of observed unique-parity states) is reproduced in Fig. 12. It is seen from Fig. 12 that parabola-like curves and, as given in Ref. 9, rotation-aligned wave functions result from a Nilsson model Coriolis calculation when the Fermi surface is at the low-K orbitals of the unique-parity shell model orbit. Inasmuch as the rotation aligned approximation appears to work rather well here, the discrepancies (noted above) with the limiting version of it for the ^{109}Pd levels are disturbing. If these discrepancies persist in the results of detailed calculations, they would constitute a significant difficulty since, as noted, the low-spin levels in ^{109}Pd occur on exactly the same footing as the high-spin levels.

To pursue this question, we have performed Nilsson model Coriolis coupling calculations, patterned exactly after those of Ref. 9, for the $h_{11/2}\otimes$rotor system in ^{109}Pd. A deformation parameter $\delta=0.15$ was used and the Fermi surface was placed at the $\frac{3}{2}^-[541]$ orbital. (This Fermi surface gave a calculated spectroscopic factor for the $\frac{11}{2}^-$ state in agreement with the experimentally observed value.) The basis states were the six isolated $h_{11/2}$ Nilsson orbitals ($\kappa=0.066$ and $\mu=0.35$). As in Ref. 9, a constant attentuation factor ($\alpha=0.8$) was applied to each Coriolis matrix element. Calculated energies were normalized to a value of 189 keV for the lowest-lying state. The best results were obtained for the modified VMI parameter $C=2\times10^7$ keV^3.

However, as already recognized in Ref. 9, the variable moments of inertia used for the low-spin states are not unambiguously defined. In Ref. 9 and in the present calculation, they were deduced by extrapolation from those for the high-spin levels. However, if indeed the variations in effective inertial parameters are due to the effects of rotation, which are similar in low- and high-spin unique-parity states, an alternate prescription might be to use moments of inertia which vary symmetrically for spins greater and less than $\frac{11}{2}$, that is, to take the inertial parameter as a function of R rather than J. However, this is also not completely realistic since it assumes a weak coupling model characterized by pure R values. In practice, several R values contribute to each state, and a larger range of R values contributes to a high-spin than to a low-spin level. Thus, for example, even though $|J-\frac{11}{2}|=4$ for both the $\frac{3}{2}^-$ and $\frac{19}{2}^-$ levels, R values of only 4 and 6 may con-

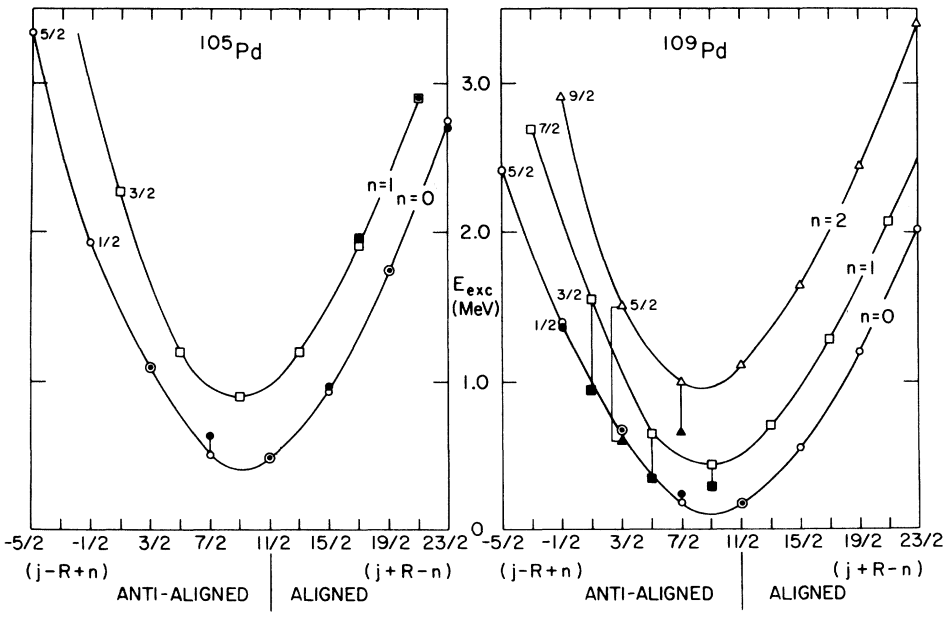

FIG. 12. Comparison of experimental (solid symbols) and calculated (open symbols) excitation energies for ^{105,109}Pd. For large differences the corresponding experimental and calculated points are connected with a vertical line. The spin of a state is given by its abscissa except as explicitly labeled for anti-aligned states with $R>j$. Values for ^{105}Pd are from Ref. 9.

tribute to the $\frac{3}{2}^-$ state (for this discussion we momentarily take the Nilsson wave functions as pure $\frac{11}{2}$ states) while $R=4$, 6, 8, 10, 12, and 14 may contribute to the $\frac{19}{2}$ level resulting in a slightly larger value for $\langle R \rangle$.

None of these prescriptions, of course, is formally correct in that the variation of the inertial parameter is derived from the final perturbed states and applied to the unperturbed states, and not derived from the structure of the initial unperturbed states entering the Coriolis calculations. Therefore, perhaps the best prescription would be one based on the actual distribution of R values in the unperturbed Nilsson wave functions. (For a more complete discussion of this approach and its inherent pitfalls, see Ref. 9.)

In any case, these questions, while of interest, ultimately have little impact on the qualitative conclusions, since in any practical calculation the adoption of a prescription for the inertial parameters is followed by an attempt to fit the empirical levels in which other parameters, in particular the Coriolis attenuation factors, are varied. Since the different inertial parameter prescriptions correspond, in effect, to an approximate scaling of one factor in the Coriolis coupling strength for the low-spin states, one is effectively forced to alter the attenuation factor to partly compensate for different coupling constants. Thus, the best fits under each prescription, though differing in detail, are very similar in overall aspect.

This is shown, for example, in the left part of Table XII in which the empirical excitation energies for ^{109}Pd are compared with calculated values for two prescriptions: Calculation I in which the rotational parameters for the unperturbed low-spin states were deduced by extrapolation as a

TABLE XII. R-component probabilities for calculated levels in ^{109}Pd.[a]

J	E_{ex} (keV) Exp.	Calc. I[b]	Calc. II[b]	Probability of final state R-component ($R \leq 10$)[c] $R=0$	2	4	6	8	10
	Favored ($n=0$) states								
$\frac{1}{2}$	1359	1393	1278	...	0.005	0.090	0.905	...	...
$\frac{23}{2}$	...	2019	1271	...	...	...	0.896	0.093	0.005
$\frac{3}{2}$	673	673	668	0.003	0.081	0.909	0.007	...	...
$\frac{19}{2}$	...	1190	752	...	...	0.879	0.111	0.004	0.004
$\frac{7}{2}$	245	190	269	0.051	0.930	0.011	0.006	0.002	
$\frac{15}{2}$	...	559	372	...	0.833	0.156	0.004	0.004	0.002
$\frac{11}{2}$	189	≡189	≡189	0.629	0.344	0.020	0.003	0.003	0.001
	Unfavored ($n=1$) states								
$\frac{3}{2}$	941	1551	1347	...	0.004	0.081	0.915	...	...
$\frac{21}{2}$	...	2073	1475	...	...	...	0.764	0.221	0.015
$\frac{5}{2}$	339	654	675	...	0.052	0.932	0.016	...	...
$\frac{17}{2}$	...	1285	986	...	...	0.695	0.280	0.025	...
$\frac{9}{2}$	287	444	514	0.002	0.703	0.282	0.013	...	...
$\frac{13}{2}$	...	710	645	...	0.533	0.406	0.060	0.001	...
	Unfavored ($n=2$) states								
$\frac{5}{2}$	604	1510	1360	...	0.001	0.074	0.910	0.015	...
$\frac{19}{2}$	...	2439	1902	...	...	0.003	0.616	0.328	0.020
$\frac{7}{2}$	645	1014	1026	...	0.038	0.888	0.070	0.004	...
$\frac{15}{2}$	...	1655	1424	...	0.061	0.477	0.418	0.041	0.001

[a] For details of how R-component probabilities are calculated see Ref. 9. Pairs of states are grouped according to their dominant R-component.

[b] Calculation I uses a spin dependent extrapolation of inertial parameters and Calculation II bases these quantities on the R structure of the unperturbed Nilsson states (see text).

[c] R components for Calculation I.

function of spin [see Eq. (19) in Ref. 9] and Calculation II in which an effective moment of inertia for each unperturbed state was obtained by summing the product of the amplitude for each R value in the Nilsson wave function and the variable moment of inertia for that R in the ^{108}Pd core. To obtain a fit comparable to that of Calculation I a somewhat unrealistic attenuation factor of unity was required in Calculation II. As is evident from the table the two calculations are similar for the experimentally known states and exhibit the same serious discrepancies with the data (see below). It is also of note that the calculated distributions of R values in the two sets of calculated wave functions for the final states are nearly identical. The effect of these various attempts to realistically represent the moments of inertia for levels with $J < \frac{11}{2}$ is to give a similar, nearly constant value of $h^2/2\mathcal{I}_K$ for each K. Thus, a Coriolis calculation using a constant rotational parameter of 40 keV and $\alpha = 0.9$ also gives results comparable to Calculation I.

The right-hand side of Fig. 12 compares the results of Calculation I with the empirical excitation energies using the format of Rekstad *et al.*[45,46] Table XII lists the probabilities for R components ($R \leq 10$) which are present in the calculated wave functions. To facilitate comparison in Table XII the states are grouped according to degree of alignment (using the convenient quantity n) and then as pairs, corresponding to the same dominant R value. Thus, for $n = 0$, the pairs of states represent the maximum anti-aligned and aligned states for a given R. It is seen from Table XII that the Nilsson model Coriolis coupling calculation results in wave functions representative of states in a rotation aligned scheme, e.g., probabilities of ~0.9 for a single R value for the favored states ($n = 0$). In fact, the degree of parallelism of $\vec{j}$ and $\vec{R}$ is even greater than at first appears for the anti-aligned states because the low-R components (e.g., $R = 0$, 2 amplitudes in the $\frac{1}{2}^-$ and $\frac{3}{2}^-$ states) must arise from full alignment of R with small $j < \frac{11}{2}$ components in the predominantly $h_{11/2}$ Nilsson wave functions, whereas R values greater than $|J - \frac{11}{2}|$ in the high-spin favored states can arise from partial nonalignment. For states that are not fully aligned or anti-aligned, the dominant R-component probability is seen to be even greater for the low-spin (anti-aligned) states than for the high-spin (aligned) states. This concentration in R space is due in part to the aforementioned fewer number of low-spin than high-spin unique-parity levels.

It is immediate evident from Fig. 12 that there are serious disagreements. Although the favored levels ($n = 0$ curve) are accurately predicted, the unfavored levels occur much lower in energy than given by the calculations and more compressed as well. In particular, one notes that there are three pairs of states with the same spin ($\frac{3}{2}$, $\frac{5}{2}$, $\frac{7}{2}$). In each pair the empirical (calculated) separations are (in keV) 268(878), 265(856), and 400(824). Overall, the discrepancies are as large as ~1 MeV for the unfavored states compared with agreement to within an average discrepancy of 30 keV for the favored states in ^{109}Pd and 65 keV for the favored states in ^{105}Pd.

As noted earlier the observed γ-ray transitions and their intensities differ appreciably from those expected for a weak coupling limit. Therefore, the parameters of Calculation I were used to calculate the intensities of the intraband $E2$ and $M1$ transitions within the framework of the Nilsson model with Coriolis coupling. Unfortunately, the comparison between calculated and observed results is limited by the fact that the multipolarities of the higher energy transitions were not measurable. For transitions of known multipolarities the calculated dominant multipolarities are in general agreement with the experimental results. For example, the 336 keV ($\frac{3}{2}^- \rightarrow \frac{5}{2}^-$) transition is calculated and measured to be $M1$, and the 94 keV ($\frac{5}{2}^- \rightarrow \frac{7}{2}^-$) transition is calculated and measured to be mixed $M1/E2$. For the 604 and 673 keV levels the intensity ratios agree with the empirical ones to within a factor of 6 in each case. The 685 keV γ ray depopulating the 1359 keV level is calculated to be predominantly $E2$, so ratios of $B(E2)$ values are considered for this level, with agreement to within a factor of 3 of the experimental results. For the 941 keV level the agreement between calculated and experimental results is poorer. The 601 and 267 keV transitions are calculated to be strongly and comparably mixed $M1/E2$, with the 601 keV transition 50–80 times more intense compared to a factor of ~8 experimentally. The calculated ratio of γ-ray intensities for the 336 keV ($M1$) and 695 keV ($E2$) transitions is ~3000. However, if an $E2$ enhancement of ~100 (see below) is included this ratio becomes ~30, in reasonable agreement with the empirical value of 10.

Empirical data[48,49] on hindrance factors in ^{103,105}Pd can be used to estimate the completeness of the level scheme for the lower-lying negative-parity states, where one might expect a strong 56 keV $E2$ transition between the $\frac{7}{2}^-$ (245 keV) and $\frac{11}{2}^-$ (189 keV) levels. For ^{103}Pd and ^{105}Pd the hindrance of $E1$ transitions depopulating the $\frac{7}{2}^-$ levels is found to be 4×10^4 and 8×10^4, respectively. In ^{105}Pd the $\frac{7}{2}^- \rightarrow \frac{11}{2}^-$ transition is enhanced by ~100. If an $E1$ hindrance of 6×10^4 and an $E2$ enhancement of 100 are assumed for ^{109}Pd, the Weisskopf estimate for the γ-ray intensity ratio

for the $\frac{7}{2}^- \rightarrow \frac{5}{2}^+$ ground state transition and the unobserved $\frac{7}{2}^- \rightarrow \frac{11}{2}^-$ transition is 270, or an absolute γ-ray intensity of 0.6 photons/1000 neutron captures for the unobserved 56 keV γ ray. An attempt was made to observe low energy γ rays with a thin intrinsic Ge detector. No 56 keV γ ray was observed for an estimated detector sensitivity of ~1.5 photons/1000 neutron captures. When corrected for internal conversion, the calculated $E2$ intensity is ~6 photons/1000 neutron captures, a value consistent with the observed population and depopulation intensities of the $\frac{11}{2}^-$ level.

The major discrepancies revealed thus far between the particle-rotor model and the data center on the level energies. These discrepancies are not an accident of the parameter values used in the calculations but are inherent in the model since they stem directly from the large Coriolis matrix elements. This is most easily seen for the two $\frac{3}{2}^-$ states. In a two state mixing calculation the minimum final separation is twice the interaction matrix element and thus, with an unattenuated Coriolis matrix element of ~500 keV, these two states *must* be calculated to be $\gtrsim$1 MeV apart, independent of their initial separation. The only recourse to lessen this separation, within the context of the model, is to attentuate the matrix element. However, with an empirical separation of 268 keV, it is clear that an attentuation factor of $\alpha \lesssim 0.25$ would be required. However, this is completely unacceptable since it gives poor overall agreement for the rest of the negative-parity levels. In fact, the lowest lying of these would then be the $\frac{3}{2}^-$, not the $\frac{11}{2}^-$ level which then occurs above *both* $\frac{3}{2}^-$ levels. This is, of course, not unexpected since Løvhøiden and Rekstad[10] have shown that the spin of the lowest-lying state in a rotation-aligned picture is given approximately by $J = \alpha[j(j+1) - 1/2]^{1/2}$.

The Nilsson model implicitly assumes an extremely truncated basis, namely that obtained by coupling the odd particle to a pure rotor or, in other words, to the ground state rotational band in the adjacent even-even nucleus. On the other hand, as noted above, rotation-aligned sequences of states are expected preeminently in weakly deformed nuclei and it is in just these nuclei where the pure rotor assumption is most suspect. One should, therefore, expect both that anharmonicities in the (quasi) ground band and that other degrees of freedom may play important roles. The use of the VMI prescription in the above calculations represents an attempt to include anharmonicities but without enlarging the basis. One common way to extend the basis has been to include axially asymmetric core shapes. In effect, this admits degrees of freedom associated with the (quasi) γ vibration and has proved to be an essential ingredient[50] in successful particle-rotor calculations in the $A = 180$–200 region.

We have, therefore, performed calculations using a triaxial (rigidly asymmetric) core with the code ASQROT written by J. Meyer-ter-Vehn.[51] The calculations were performed for several values of the deformation parameter β ($\beta \simeq 1.06\delta$) in the range 0.15–0.35, including the values which would be obtained from the energies of the first 2^+ states in the adjacent even-A Pd nuclei. The Fermi surface was placed at the $\frac{3}{2}^-$ [541] Nilsson orbital for direct comparison of results with the previous calculations.

The calculations lead to plots similar to those in Ref. 51. From them we have extracted the energy differences between the lowest two $\frac{3}{2}^-$ and lowest two $\frac{5}{2}^-$ states. The results are plotted in Fig. 13 for two different deformations. One sees that the introduction of asymmetry is of essentially no help. Even for the unrealistically large deformation of $\beta = 0.31$ the separations remain generally much larger than the empirical ones.

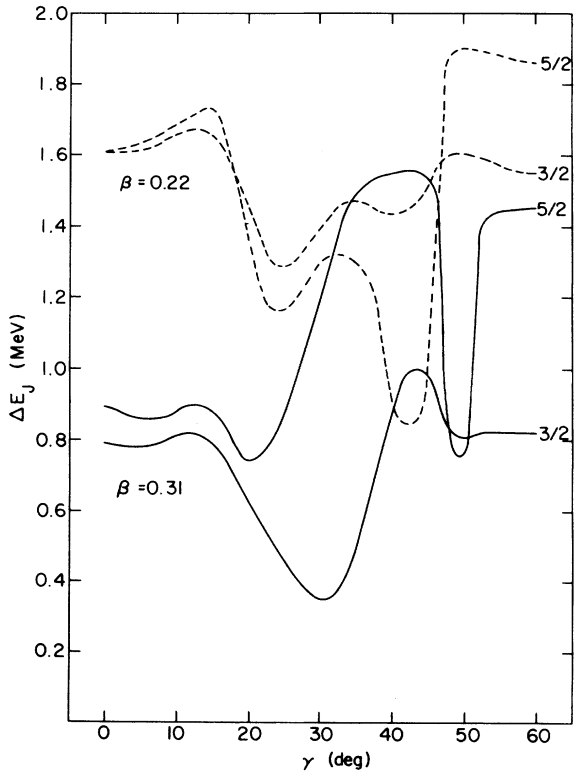

FIG. 13. The energy separation (ΔE_J) between states of the same spin ($\frac{3}{2}, \frac{5}{2}$) as calculated for an $h_{11/2}$ neutron coupled to an asymmetric core with $\beta = 0.22$ and $\beta = 0.31$. For $A = 109$ the dashed curve corresponds to $\beta A^{2/3} = 5$ and the solid curve $\beta A^{2/3} = 7$.

At $\gamma \sim 30°$, though the $\frac{3}{2}^-$ separation drops to ~400 keV, the separation in the $\frac{5}{2}^-$ states is >1 MeV. For more reasonable (smaller) deformations than shown the separations are still larger.

It therefore appears that there are more serious difficulties with the particle-rotor model. Whether these could be removed by the introduction of further degrees of freedom is currently unclear, as are the questions of whether it is primarily the unfavored levels that are susceptible to such refinements or if the difficulty somehow, unexpectedly, centers on the low-spin states, or whether the usual agreement for high-spin aligned states is perhaps fortuitous. If nonground band core amplitudes are, in fact, important, they would lead to the presence of additional low-spin negative-parity levels, the search for which might provide a sensitive probe. The only likely candidate among the levels in Fig. 8 would seem to be the 1134 keV $\frac{1}{2}^-, \frac{3}{2}^+$ level which does seem to preferentially feed the unique-parity sequence of states. Preliminary calculations,[52] reported elsewhere, suggest that one can account for the empirical negative-parity levels in the framework of the newly developed interacting boson approximation for odd mass nuclei.[53] A full and proper discussion of this, however, is best reserved for a subsequent publication.

IV. SUMMARY

A thorough study of the (n,γ) and $(n,\gamma ce)$ reactions on ^{108}Pd has been made to determine level spin parities in ^{109}Pd. A number of J^π values have been more firmly established and important discrepancies with earlier work have emerged.

The new spin values have been used to obtain revised spectroscopic factors and spectroscopic factor sums in ^{109}Pd. As a result the study has suggested a resolution of the $g_{7/2}$-$h_{11/2}$ anomaly for the ^{109}Pd by demonstrating previous misassignments for several levels. ^{107}Pd now stands alone in this region in exhibiting an unusually empty $g_{7/2}$ orbit and two strong low-lying $\frac{7}{2}^+$ states. Our discussion suggests that one of these $\frac{7}{2}^+$ assignments may be incorrect or incomplete (e.g., corresponds to an unresolved doublet in the charged particle spectra). The apparent fullness of the $h_{11/2}$ orbit in the Ru and Pd nuclei is most likely an artifact of the existence of undetected $\frac{11}{2}^-$ levels at higher excitation energies.

The present work also discloses a family of unique-parity low-spin states built upon the $\frac{11}{2}^-$ state at 189 keV. In the context of a particle plus rotor description, these states correspond to the anti-alignment of the angular momentum of an $h_{11/2}$ particle with the rotational angular momentum of an even-A rotor and are thus the low-spin counterparts of the high-spin states populated in heavy-ion reactions. This is the first time that such a full set of favored and unfavored anti-aligned levels, including three with $R > j$, has been observed. Since a Nilsson model Coriolis coupling calculation has successfully reproduced high-spin states of this type in the $A \sim 100$ region and can lead to rotation-aligned spectra, it should be able to also describe the low-spin states. It is found that this model is unable to reproduce the energies of the unfavored states. Furthermore, introducing extra degrees of freedom in the core via an asymmetric rotor does not improve the description.

Contrary to the situation for normal-parity levels, unique-parity states are equally isolated regardless of whether they have low or high spin. One therefore expects the particle-rotor model to work as well for low- as for high-spin states. Thus, the present results suggest that unless and until it is understood whether the difficulties encountered reveal a general problem with the particle-rotor model or whether there is indeed some as yet unrecognized property that localizes the discrepancies in the low-spin states, one should exercise renewed caution in assessing the apparent success the particle-rotor model seems to enjoy in generating rotation-aligned spectra for the subset of high-spin aligned levels usually observed. They further argue strongly for additional efforts to observe other sets of low-spin anti-aligned states in order that the expanded systematics so generated will reveal more completely the extent, in spin, excitation energy, and nucleus, of the discrepancies with the particle-rotor scheme and perhaps lead to a resolution of the difficulties either by illuminating the limitations of the model or by suggesting refinements in it.

ACKNOWLEDGMENTS

We are grateful to Doctor F. A. Rickey and Doctor H. A. Smith for numerous valuable discussions and in particular to the former for discussions of the VMI prescriptions for low-spin states and to both for providing the computer code CORCUP. We also thank J. Meyer-ter-Vehn for providing the code ASQROT. We acknowledge useful discussions with Dr. D. D. Warner. This work was performed under Contract No. EY-76-C-02-0016 with the Division of Basic Energy Sciences, U.S. Department of Energy.

*Present address: United Kingdom Atomic Authority, Cheshire, England WA3 GAT.
†Present address: Universität Ulm, 7900 Ulm, West Germany.
‡Present address: Los Alamos Scientific Laboratory, Los Alamos, New Mexico 87545.

[1]B. I. Cohen, J. B. Moorhead, and R. A. Moyer, Phys. Rev. 161, 1257 (1967).
[2]R. C. Diehl, B. L. Cohen, R. A. Moyer, and L. H. Goldman, Phys. Rev. C 1, 2086 (1970); Phys. Rev. 180, 1210 (1969).
[3]B. L. Cohen, R. A. Moyer, J. B. Moorhead, L. H. Goldman, and R. C. Diehl, Phys. Rev. 176, 1401 (1968).
[4]F. S. Stephens, R. M. Diamond, and S. G. Nilsson, Phys. Lett. 44B, 429 (1973); F. S. Stephens, Rev. Mod. Phys. 47, 43 (1975).
[5]P. C. Simms, G. J. Smith, F. A. Rickey, J. A. Grau, J. R. Tesmer, and R. M. Steffen, Phys. Rev. C 9, 684 (1974).
[6]J. A. Grau, F. A. Rickey, G. J. Smith, P. C. Simms, and J. R. Tesmer, Nucl. Phys. A229, 346 (1974).
[7]F. A. Rickey, J. A. Grau, L. E. Samuelson, and P. C. Simms. Phys. Rev. C 15, 1530 (1977).
[8]W. Klamra and J. Rekstad, Nucl. Phys. A258, 61 (1976).
[9]H. A. Smith, Jr. and F. A. Rickey, Phys. Rev. C 14, 1946 (1976).
[10]G. Løvhøiden and J. Rekstad, Phys. Lett. 60B, 335 (1976), and references cited therein.
[11]T. L. Khoo, F. M. Bernthal, C. L. Dors, M. Piiparinen, S. Saha, P. J. Daly, and J. Meyer-ter-Vehn, Phys. Lett. 60B, 341 (1976).
[12]H. H. Güven, B. Kardon, and H. Seyfarth, Z. Phys. A287, 271 (1978).
[13]S. F. Mughabghab, W. R. Kane, and R. F. Casten, in *Nuclear Structure Study with Neutrons*, proceedings of a conference in Budapest, Hungary, 31 July–5 August, 1972, edited by J. Erö and J. Szücs (Hungarian Academy of Sciences, Budapest, Hungary, 1974), p. 484.
[14]G. J. Smith, R. F. Casten, M. L. Stelts, H. G. Börner, W. F. Davidson, and K. Schreckenbach, Phys. Lett. 86B, 13 (1979).
[15]F. E. Bertrand, Nucl. Data Sheets 6, 1 (1971), and references cited therein.
[16]G. Franz, Annual Report, University of Mainz, 1975.
[17]M. Kanazawa, S. Ohya, T. Tamura, Z. Matumoto, and N. Mutsuro, J. Phys. Soc. Japan 44, 25 (1978); P. Fettweis and P. del Marmol, Z. Phys. A275, 359 (1975).
[18]W. R. Kane, D. Gardner, T. Brown, A. Kevey, E. der Mateosian, G. J. Emery, W. Gelletly, M. A. J. Mariscotti, and I. Schröder, *Proceedings of the International Symposium on Neutron Capture Gamma Ray Spectroscopy, Studsvik, August, 1969* (International Atomic Energy Agency, Vienna, 1969), p. 105.
[19]*Neutron Cross Sections*, compiled by S. F. Mughabghab and D. I. Garber, Brookhaven National Laboratory Report No. BNL-325 (National Technical Information Service, Springfield, Virginia, 1973), 3rd edition, Vol. 1.
[20]F. E. Bertrand, Nucl. Data Sheets 23, 229 (1978), and references cited therein.
[21]N. C. Rasmussen, V. J. Orphan, Y. Hukai, and T. Inouye, Nucl. Data A3, 626 (1967).
[22]J. E. Rambak and E. Steinnes, private communication.
[23]M. L. Stelts and R. E. Chrien, Nucl. Inst. and Math. 155, 253 (1978); R. C. Greenwood and R. E. Chrien, Nucl. Instrum. Methods 138, 125 (1976).
[24]H. Börner *et al.*, in *Proceedings of the Second International Symposium on Neutron Capture Gamma-ray Spectroscopy and Related Topics, Petten, The Netherlands, 1974,* edited by K. Abrahams *et al.* (Energy Centrum Nederland, Petten, The Netherlands, 1975), p. 691; H. R. Koch, Jül. Spez-10, KFA Jülich report, 1978.
[25]R. G. Helmer, R. C. Greenwood, and R. J. Gehrke, Nucl. Instrum. Methods 155, 189 (1975).
[26]W. Mampe, K. Schreckenbach, P. Jeuch, B. P. K. Maier, F. Braumandl, J. Larysz, and T. von Egidy, Nucl. Instrum. Methods 154, 127 (1978).
[27]R. S. Hager and E. C. Seltzer, Nucl. Data A4, 1 (1968).
[28]L. M. Bollinger and G. E. Thomas, Phys. Rev. C 2, 1951 (1970); Phys. Rev. Lett. 18, 1143 (1967); 21, 233 (1968).
[29]A. M. Lane and J. E. Lynn, Nucl. Phys. 17, 586 (1960).
[30]J. E. Lynn, *The Theory of Neutron Resonance Reactions* (Clarendon, Oxford, England, 1968).
[31]A. M. Lane and S. F. Mughabghab, Phys. Rev. C 10, 412 (1974).
[32]S. F. Mughabghab, R. E. Chrien, O. A. Wasson, G. W. Cole, and M. H. Bhat, Phys. Rev. Lett. 26, 1118 (1971).
[33]S. F. Mughabghab, in *Nuclear Structure Study with Neutrons*, proceedings of a conference in Budapest, Hungary, 31 July–5 August, 1972, edited by J. Erö and J. Szücs (Hungarian Academy of Sciences, Budapest, Hungary, 1974), p. 167.
[34]S. F. Mughabghab, in *Proceedings of the Second International Symposium on Neutron Capture Gamma-ray Spectroscopy and Related Topics, Petten, The Netherlands, 1974*, edited by K. Abrahams *et al.* (Energy Centrum Nederland, Petten, The Netherlands, 1975), p. 53.
[35]O. A. Wasson and G. C. Slaughter, Phys. Rev. C 8, 297 (1973).
[36]J. W. Boldeman, B. J. Allen, A. R. del Musgrove, and R. L. Macklin, Nucl. Phys. A246, 1 (1975).
[37]H. T. Fortune, G. C. Morrison, J. A. Nolen, Jr., and P. Kienle, Phys. Rev. C 3, 337 (1971).
[38]P. Maier-Komer, P. Glässel, E. Huenges, H. J. Scheerer, H. K. Vonach, and H. Baier, Z. Phys. A278, 327 (1976).
[39]F. A. Rickey, R. E. Anderson, and J. R. Tesmer, report.
[40]J. B. Moorhead, B. L. Cohen, and R. A. Moyer, Phys. Rev. 165, 1287 (1968).
[41]P. E. Cavanagh, C. F. Coleman, A. G. Hardacre, G. A. Gard, and J. F. Turner, Nucl. Phys. A141, 97 (1970).
[42]E. J. Schneid, Arand Prakash, and B. L. Cohen, Phys. Rev. 156, 1316 (1967).
[43]M. J. Bechara and O. Dietsch, Phys. Rev. C 12, 90 (1975).
[44]T. Borello-Lewin, C. Q. Orsini, O. Dietsch, and E. W. Hamburger, Nucl. Phys. A249, 284 (1975).
[45]J. Rekstad, E. Osnes, and T. Engeland, in *Proceedings of the International Conference on Nucl. Structure, Tokyo, 1977* (Phys. Soc. of Japan, Tokyo, 1977), contributed papers, p. 99.
[46]T. Pederson and E. Osnes, Nucl. Phys. A303, 345

(1978).
[47]M. A. J. Mariscotti, G. Scharff-Goldhaber, and B. Buck, Phys. Rev. 178, 1864 (1969).
[48]W. Dietrich, B. Nyman, A. Johansson and A. Bäcklin, Phys. Scr. 12, 80 (1975).
[49]C. M. Lederer and V. S. Shirley, *Table of Isotopes*, seventh edition (Wiley, New York, 1978), and references cited therein.
[50]See, for example, S. K. Saha, M. Piiparinen, J. C. Cunnane, P. J. Daly, C. L. Dors, T. L. Khoo, and F. M. Bernthal, Phys. Rev. C 15, 94 (1977).
[51]J. Meyer-ter-Vehn, Nucl. Phys. A249, 111 (1975).
[52]R. F. Casten and G. J. Smith, Phys. Rev. Lett. 43, 337 (1979).
[53]F. Iachello and O. Scholten, Phys. Rev. Lett. 43, 679 (1979), and private communication.